1. Introduction

Cyclic AMP response element-binding protein (CREB) is a transcription factor (Brindle and Montminy, 1992) that was originally shown to be phosphorylated at serine residue 133 (Ser-133) by an activated cAMP-dependent protein kinase A and mitogen activated protein kinases (MAPKs). The phosphorylation of this residue allows the recruitment of CREB-binding protein (CBP) or its paralogue, p300 (Johannessen et al., 2004; Roach et al., 2005). CREB regulates responses to growth factors, inflammatory mediators, and some cell-activating agents by binding to cAMP response elements (CRE) (Caivano and Cohen, 2000; Liu et al., 2004; Ma and Eisenach, 2002; Mayr and Montminy, 2001). The phosphorylation of CREB participates in a wide range of cellular events in the nervous system, including neuronal differentiation (Bender et al., 2001), neuronal survival (Ryu et al., 2005), neuropathic pain (Ma and Quirion, 2001), and inflammation (Etienne-Manneville et al., 1999). Little is known about the phosphorylation of CREB in autoimmune central nervous system (CNS) disease models such as experimental autoimmune encephalomyelitis (EAE), which is characterized by reactive gliosis as well as infiltration of autoimmune T and bystander cells (Schonrock et al., 1998; Shin et al., 1995, 2003).

Our previous studies have shown that the MAPK pathway, which is upstream of CREB, is activated in autoimmune inflammation in the nervous system (Ahn et al., 2004; Moon et al., 2005; Shin et al., 2003) and that the resulting pro-inflammatory cytokines are associated with the induction of EAE paralysis (Tanuma et al., 1997). These factors are associated with the activation of CREB in each cell type.

The aim of the present study was to determine whether CREB is implicated in the course of EAE, which is an animal model of human multiple sclerosis.

2. Results

2.1. Clinical progression of experimental autoimmune encephalomyelitis and histopathological findings

EAE-affected rats immunized with myelin basic protein (MBP) developed floppy tails (grade 1, G.1) on days 9-11 post-immunization (p.i.) and exhibited progressive hind limb paralysis (G.2 or G.3) on days 12-14 p.i. All of the rats recovered on day 21 p.i. (recovery 0, R.0).

Histopathological examination showed no infiltrating cells in the spinal cord of the normal controls (Fig. 1A). With hind limb paralysis, inflammatory cells infiltrated the parenchyma of the spinal cord in EAE-affected rats (day 12 p.i.; Fig. 1B). In the EAE lesions, most of the inflammatory cells were ED1-positive macrophages (Fig. 1C) and monoclonal anti-T cell receptor $\alpha\beta$ (R73)-positive T cells (Fig. 1D). The clinical observations and histological findings related to EAE largely corresponded to those described previously (Shin et al., 1995, 2003).
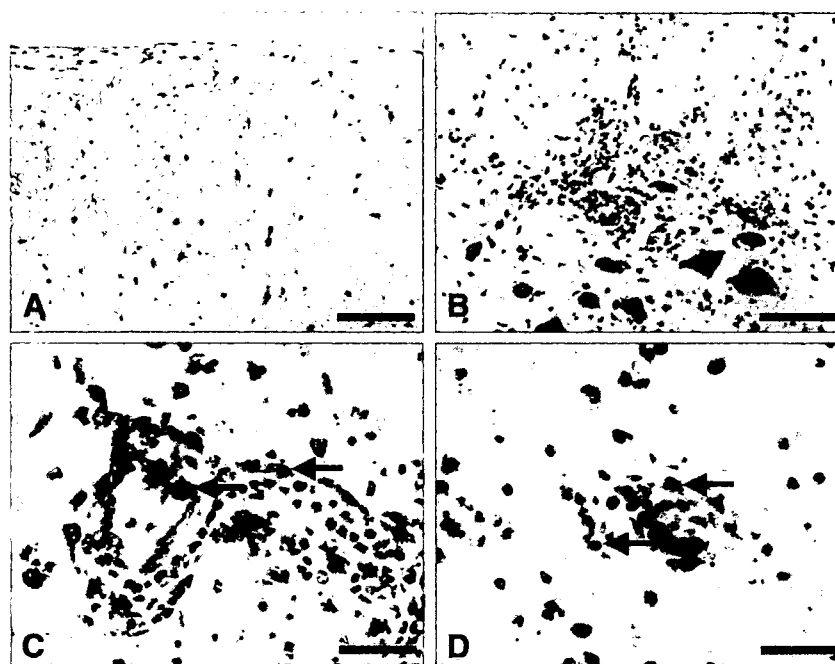

Fig. 1 - Histopathological examination of normal and EAE-affected rat spinal cords. (A) There are no inflammatory cells in the spinal cords of the normal control rats. (B) On day 12 after the injection of myelin basic protein, many inflammatory cells are present in the spinal cord of EAE-affected rats. (C, D) The majority of the inflammatory cells within the EAE lesions are ED1-positive macrophages (C, arrows) and R73 (TCR $\alpha\beta$)-positive T cells (D, arrows). A and B: hematoxylin-eosin staining. C and D: immunostained with either ED1 (C) or R73 (D) and counterstained with hematoxylin. Scale bars: in panels A and B, 80 μm; in panels C and D, 40 μm.

2.2.   Activation of CREB and ATF-1 in the spinal cord in EAE

Antibody to the phosphorylated form of CREB (p-CREB) detects endogenous levels of CREB only when CREB is phosphorylated at Ser-133 and also detects the phosphorylated form of CREB-related protein activating transcription factor-1 (p-ATF-1). Therefore, we used different normalized bands for the analysis of p-CREB and p-ATF-1; the intensity of p-CREB was normalized to CREB, and the intensity of p-ATF-1 was normalized to beta-actin.

The level of p-CREB in the spinal cord was semiquantitatively evaluated during the course of EAE, using Western blot analysis. The expression of p-CREB immunoreactivity was detected at low levels in the spinal cord of normal control rats (density, 0.35 ± 0.06 OD/mm^2; $n=5$); it significantly increased in the spinal cord during the peak stage of EAE (G.3, day 12 p.i.; 1.57 ± 0.15 OD/mm^2; $n=5$; $p<0.05$ vs. controls) and subsequently declined in the recovery stage (R.0, day 21 p.i.; 0.34 ± 0.07 OD/mm^2; $n=5$; $p<0.05$ vs. peak stage of EAE) (Fig. 2).

The expression of p-ATF-1 immunoreactivity was also detected at low levels in the spinal cord of normal control rats (0.26 ± 0.04 OD/mm^2; $n=5$); it significantly increased in the spinal cord in the peak stage of EAE (G.3, day 12 p.i.; 0.84 ± 0.13 OD/mm^2; $n=5$; $p<0.05$ vs. controls). The expression was

slightly lower in the recovery stage of EAE (R.0, day 21 p.i.; 0.53 ± 0.1 OD/mm^2; $n=5$) but was still higher than the control level ($p<0.05$ vs. controls) (Fig. 2).

2.3.   Localization of p-CREB in spinal cord sections from EAE-affected rats

2.3.1.   p-CREB immunoreactivity

Immunohistochemically, p-CREB was detected in a few glial cells in the normal rat spinal cord (Fig. 3A). In the peak stage of EAE (G.3, day 12 p.i.), many p-CREB-positive glial cells were detected in the white (Fig. 3B) and gray (data not shown) matter of the spinal cord. In addition, during the peak stage of EAE, there was massive infiltration of inflammatory cells in the parenchyma, where some round cells were positive for p-CREB (Fig. 3C). In the recovery stage of EAE (R.0, day 21 p.i.), there were fewer inflammatory cells than in the peak stage, and a few glial cells were positive for p-CREB (Fig. 3D).

In addition, p-CREB was detected in neurons in the dorsal horn lamina of the normal rat spinal cord (mean number ± SEM: 39.57 ± 7.62) (Fig. 4A). In the peak stage of EAE (G.3, day 12 p.i.), p-CREB-positive neurons in the dorsal horn lamina were increased compared with normal control rats (66.57 ± 7.62; $p<0.05$ vs. controls) (Fig. 4B); the immunoreactivity decreased
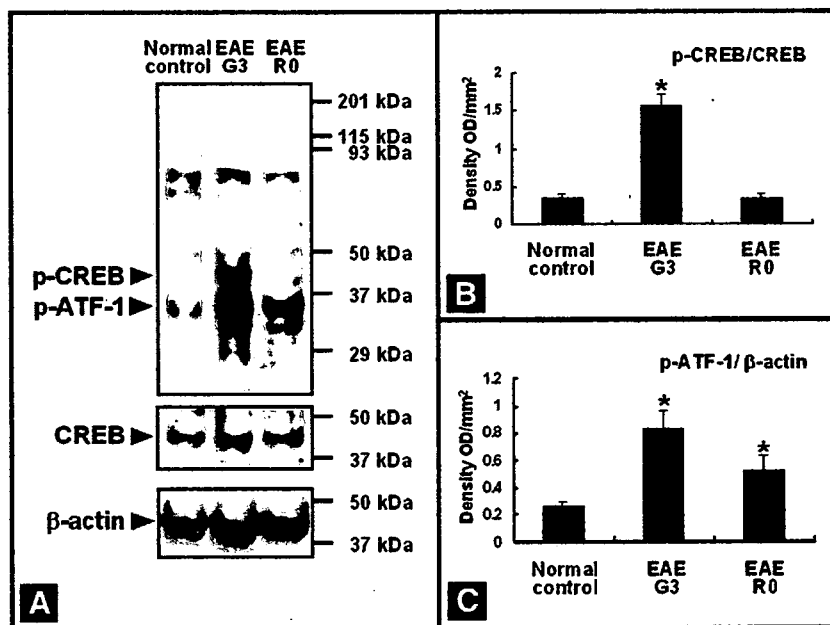
Fig. 2 – Western blot analysis of p-CREB and p-ATF-1 expression in the spinal cord of rats with EAE. Spinal cord samples were collected from normal control rats, rats at the peak stage of EAE (day 12 p.i.; stage G.3), and rats during the recovery stage (day 21 p.i.; stage R.0). (A) Representative photographs of Western blots; arrowheads indicate the expression of p-CREB (~43 kDa), p-ATF-1 (~35 kDa), CREB (~43 kDa), and beta-actin (~45 kDa). (B) Semiquantitative analysis of p-CREB immunoreactivity in spinal cords, normalized to the intensity of CREB expression in the same immunoblot. The p-CREB expression is significantly greater in spinal cords from rats sacrificed at the peak of EAE (G.3, $p<0.05$) than in spinal cords from control rats, and the expression level declines to control levels during the recovery stage (R.0) from EAE. Data (mean ± SEM) are from five experiments. *$p<0.05$ vs. normal controls and the recovery stage of EAE. (C) Semiquantitative analysis of p-ATF-1 immunoreactivity in spinal cords, normalized to the intensity of beta-actin expression in the same immunoblot. p-ATF-1 is detected in the normal controls, and its expression is significantly increased in EAE-affected spinal cords. *$p<0.05$ vs. normal controls.
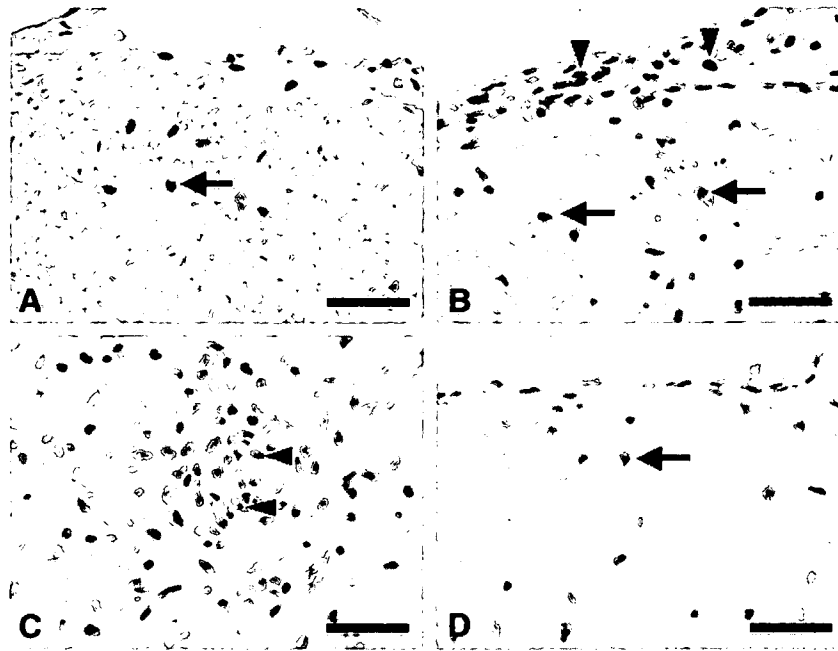
Fig. 3 – Immunohistochemical staining of p-CREB in the spinal cords of normal control rats (A) and rats at the peak (day 12 p.i.) (B, C) and recovery stages of EAE (day 21 p.i.) (D). (A) p-CREB is weakly detected in some glial cells (arrow) in the spinal cord of normal control rats. (B, C) In the peak stage of EAE, glial cells show increased immunoreactivity for p-CREB (B, arrows), and p-CREB-positive inflammatory cells are detected in the subarachnoid space (B, arrowheads) and parenchyma (C, arrowheads). (D) In the recovery stage of EAE, some p-CREB immunoreactive cells remain (arrow). Counterstained with hematoxylin. Scale bars: 40 μm.
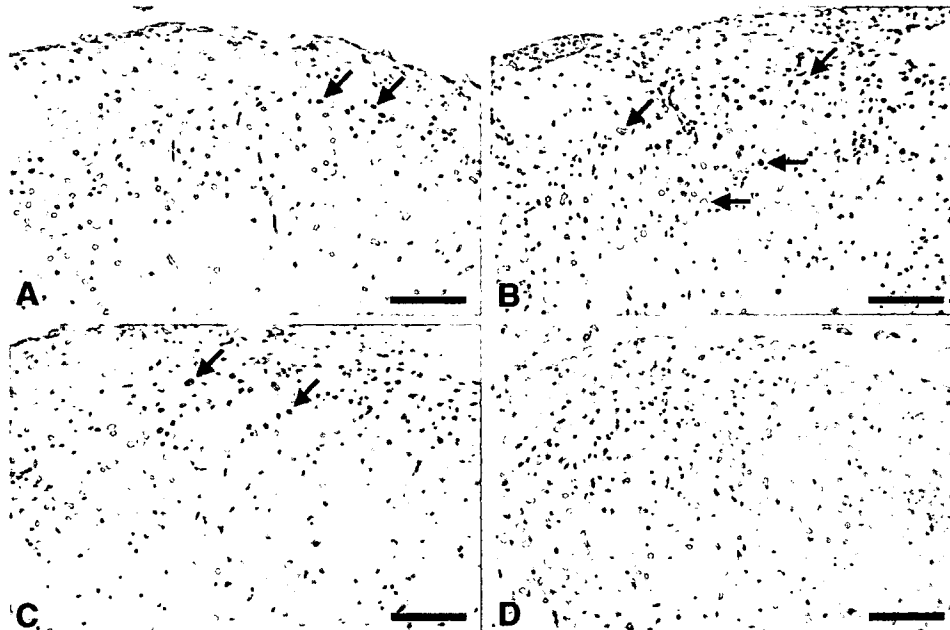

Fig. 4 – Immunohistochemical staining of p-CREB in the dorsal horn lamina in the spinal cords of normal control rats (A) and rats at the peak (day 12 p.i.) (B) and recovery stages of EAE (day 21 p.i.) (C). (A) p-CREB is constitutively immunostained in the dorsal horn lamina in the normal controls. (B, C) The p-CREB immunoreactivity is significantly increased in the dorsal horn lamina in the peak stage (B) and has declined in the recovery stage of EAE (C). (D) Tissue from a rat in the peak stage of EAE stained without primary antisera shows no staining. Counterstained with hematoxylin. Scale bars: 100 μm.
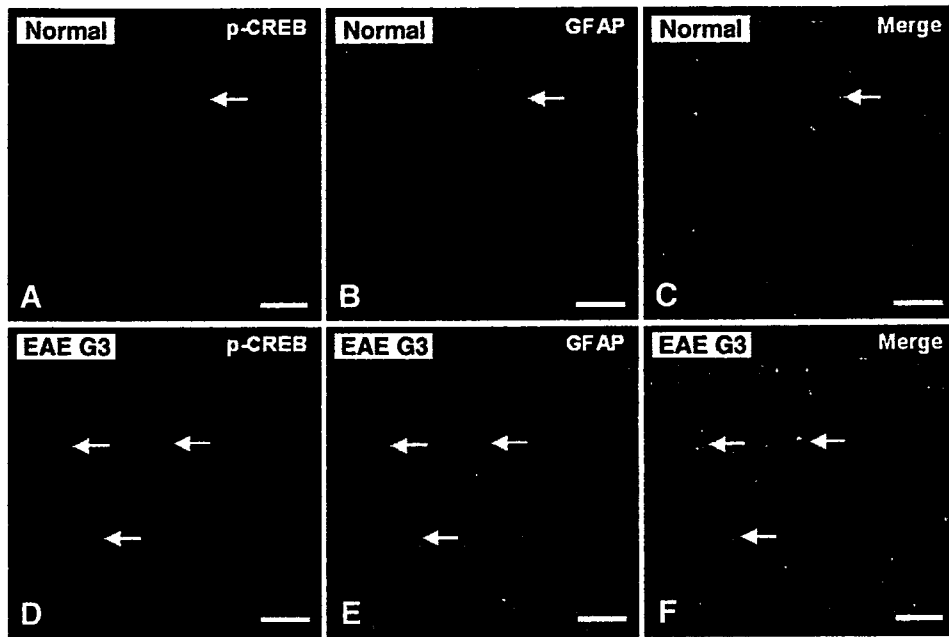
Fig. 5 – Immunofluorescent co-localization of p-CREB (A, D; red) with anti-GFAP (B, E; green) in the spinal cords of normal control rats (A–C) and rats at the peak stage of EAE (day 12 p.i.) (D–F). (A–C) In the normal controls, some p-CREB-immunopositive glial cells are co-localized in GFAP-positive astrocytes in the spinal cords (arrows). (D–F) In the EAE-affected spinal cords, many p-CREB-positive glial cells were positive for GFAP (arrows). C and F are merged images. Scale bars: 50 μm.

significantly in the recovery stage of EAE (43.86 ± 5.2; $p < 0.05$ vs. peak stage of EAE) (Fig. 4C). Some p-CREB-positive ependymal cells were detected in the spinal cords of normal control rats and rats with EAE (data not shown).

2.3.2. Identification of p-CREB-positive cells in the spinal cords of normal controls and rats with EAE

The patterns of p-CREB immunofluorescence in the spinal cords of normal control rats and rats with EAE were similar to those seen with single immunoperoxidase staining (Figs. 3 and 4). Very little p-CREB (Fig. 5A, red) was immunodetected in GFAP-positive-astrocytes (Fig. 5B, green) in the control spinal cord (Fig. 5C, merge). In the EAE spinal cord (day 12 p.i.), p-CREB-positive astrocytes increased (Figs. 5D–F). p-CREB

(Fig. 6A, red) was abundant in ED1-positive cells (Fig. 6B, green; Fig. 6C, merge), suggesting that the majority of macrophages were positive for p-CREB in EAE lesions at the peak stage.

3.   Discussion

This study is the first to show that a gene transcription factor, CREB, is phosphorylated in host and inflammatory cells in the spinal cord of animals with EAE, particularly during the peak stage, suggesting that CREB phosphorylation is closely associated with autoimmune inflammatory attack in the spinal cord.
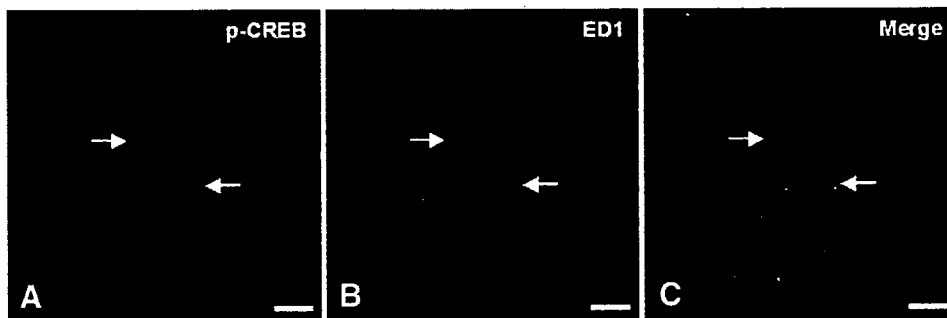

Fig. 6 – Immunofluorescent co-localization of p-CREB (A) with ED1 (B) in the spinal cord of rats in the peak stage of EAE (day 12 p.i.). A large amount of p-CREB (A, red; arrows) was immunostained in ED1-positive macrophages (B, green; arrows) (C, merge; arrows). Scale bars: in A–C, 20 μm.

With regard to the phosphorylation of CREB in the peak stage of EAE, the activation of CREB has been associated with signal enzymes such as MAPKs (Shin et al., 2003) as well as pro-inflammatory cytokines, including interferon-γ (IFN-γ) and tumor necrosis factor-α (TNF-α) (Renno et al., 1995; Tanuma et al., 1997). The MAPKs transduce a variety of extracellular stimuli through a cascade of protein phosphorylation, leading to the activation of gene transcription factors (Seger and Krebs, 1997). Two potential in vivo substrates for the MAPK pathway are CREB and the closely related ATF-1. MAPKs phosphorylate CREB at Ser-133 (Johannessen et al., 2004). Moreover, several further lines of evidence are consistent with the hypothesis that CREB and ATF-1 become phosphorylated at the relevant sites in response to growth factors, inflammatory mediators, and some cell-activating and -damaging stimuli (Caivano and Cohen, 2000; Kingsley-Kallesen et al., 1999; Zaman et al., 1999). This study confirms that the phosphorylation of CREB in EAE lesions occurs in the inflammatory cells, astrocytes, and neurons, which corresponds to the increased phosphorylation of MAPKs in rats with EAE as reported in our previous study (Shin et al., 2003). Thus, we postulate that the activation of MAPKs affects the phosphorylation of CREB in affected cells in the spinal cord with EAE through the activation of CREB and ATF-1 signaling pathways.

In response to stimuli, macrophages undergo a series of processes such as chemotaxis, phagocytosis, and the release of inflammatory mediators (Rotshenker, 2003). IFN-γ has been shown to activate the CREB signaling pathway in murine peritoneal macrophages (Liu et al., 2004), and the activation of CREB/ATF-1 promotes the production of pro-inflammatory cytokines such as TNF-α and interleukin-1β (IL-1β) in lipopo-lysaccharide (LPS)-stimulated macrophages (Caivano and Cohen, 2000). The inflammatory mediators (IFN-γ and TNF-α) described above have been closely associated with EAE lesions (Renno et al., 1995; Tanuma et al., 1997). Considering the data obtained from the present study, we postulate that pro-inflammatory cytokines, including IFN-γ, activate ED1-positive macrophages with an increased phosphorylation of CREB, possibly leading to the further production of pro-inflammatory cytokines, including TNF-α.

With regard to the inflammatory stimuli involved in the phosphorylation of CREB in astrocytes, which are an important cell type in EAE, it is known that LPS induces an increase in CREB phosphorylation via the MAPK pathway in cultured astrocytes (Buzas et al., 2002). In addition, LPS has been associated with the induction of IL-1 and TNF-α in cultured human astrocytes (Velasco et al., 1991). In the present study, we found that the phosphorylation of CREB increased in reactive astrocytes in the peak stage of EAE, suggesting that CREB activation may be involved in the gene transcription of inflammatory mediators in autoimmune-stimulated astrocytes as well as in macrophages.

Although the phosphorylation of CREB has been immuno-detected at intense levels in macrophages and astrocytes in EAE, it was also found in the dorsal horn neurons in the peak stage of EAE in the present study. This finding implies that increased phosphorylation of CREB plays an important role in the sensory function during the course of EAE. There is a general consensus that the phosphorylation of CREB in dorsal horn neurons is possibly involved in the generation and maintenance of neuropathic pain caused by partial sciatic nerve ligation (Ma and Quirion, 2001) and spinal cord injury (Crown et al., 2006).

It was recently shown that, in both active and passive EAE, there was an initial increase in tail withdrawal latency (hypoalgesia) that peaked several days prior to the peak in motor deficits during the acute disease phase (Aicher et al., 2004). Considering these results, it is highly possible that increased CREB phosphorylation in the dorsal horn neurons in the spinal cord of rats with EAE leads to the generation and maintenance of neuropathic pain.

When all the findings are taken into consideration, they suggest that increased phosphorylation of CREB occurs in the spinal cord in the peak stage of EAE and contributes to the activation of inflammatory cells such as macrophages, to the occurrence of reactive astrogliosis, and partially to the generation of neuropathic pain during the course of rat EAE and possibly in human multiple sclerosis.

4. Experimental procedures

4.1. Animals

Lewis rats were obtained from Harlan (Indianapolis, IN) and were bred in our animal facility. Male rats (7-8 weeks old; 160-200 g) were used in this study. All experiments followed accepted ethical guidelines.

4.2. Induction of experimental autoimmune encephalomyelitis

The footpads of both hind feet of rats in the EAE group were injected with 100 μl of an emulsion that contained equal parts of MBP (1 mg/ml) and complete Freund's adjuvant (CFA) supplemented with Mycobacterium tuberculosis H37Ra (5 mg/ml) (Difco, Detroit, MI). Control rats were immunized with CFA only. After immunization, the rats were observed daily for clinical signs of EAE. The progression of EAE was divided into seven clinical stages: Grade 0 (G.0), no signs; G.1, floppy tail; G.2, mild paraparesis; G.3, severe paraparesis; G.4, tetrapar-esis; G.5, moribund condition or death; and R.0, recovery (Shin et al., 1995).

4.3. Antibodies

Rabbit polyclonal anti-p-CREB (Ser-133) and anti-CREB antibodies were obtained from Cell Signaling Technology (Beverly, MA). The p-CREB antibody also detects the phosphorylated form of CREB-related protein ATF-1 (as characterized by the manufacturer). Mouse monoclonal anti-beta-actin and mouse anti-GFAP were obtained from Sigma (St. Louis, MO). ED1 (mouse monoclonal anti-rat macrophages) was obtained from Serotec (London, UK). R73 (mouse monoclonal anti-T cell receptor αβ) was obtained from Blackthorn (Bicester, Bucks, UK).

4.4. Tissue sampling

The rats were sacrificed under ether anesthesia. The spinal cords were dissected from each group at 12-14 and 21 days p.i.

($n=5$ rats/group); these periods coincided with the peak (G.3, day 12–14 p.i.) and recovery (R.0, day 21 p.i.) stages of EAE. Samples of the spinal cords were processed for embedding in paraffin wax after fixation in 4% paraformaldehyde in phosphate-buffered saline (PBS, pH 7.4). Paraffin sections (5 μm thick) were used for all immunostaining, except for the T cell marker R73. For T cell immunostaining, pieces of the spinal cords were snap-frozen in optimal cutting temperature compound (Sakura, Tokyo, Japan), and sections (8 μm thick) were cut using a cryostat (Leica, Nussloch, Germany). Additional spinal cord samples were snap-frozen and stored for immunoblot analysis.

4.5. Western blot analysis

The spinal cord tissue was homogenized in modified radio-immunoprecipitation assay (RIPA) buffer (20 mM Tris, pH 7.5, 150 mM NaCl, 1% Triton-X 100, 0.5% sodium deoxycholate, 0.1% sodium dodecyl sulfate, 1% NP-40, 10 mM NaF, 1 mM EDTA, 1 mM EGTA, 1 mM Na_3VO_4, 1 mM PMSF, 10 μg/ml aprotinin, and 10 μg/ml leupeptin) with 20 strokes in a homogenizer. The homogenate was transferred to microtubes and centrifuged at 14,000 rpm for 20 min, and the supernatant was harvested.

For the immunoblot assay, supernatant samples containing 40 μg of protein each were loaded into individual lanes of 10% sodium dodecyl (lauryl) sulfate-polyacrylamide gels, electrophoresed, and immunoblotted onto nitrocellulose membranes (Schleicher and Schuell, Keene, NH). The residual binding sites on the membrane were blocked by incubation with 5% nonfat milk in Tris-buffered saline (TBS; 10 mM Tris–HCl, pH 7.4, and 150 mM NaCl) for 1 h. Subsequently, the membrane was incubated for 2 h with rabbit polyclonal anti-p-CREB (1:1000 dilution) antibody. The membranes were washed three times in TBS containing 0.1% Tween 20 and then incubated with horseradish peroxidase-conjugated anti-rabbit IgG (Vector, Burlingame, CA) for 1 h. Bound antibodies were detected using chemiluminescent substrate (WEST-one™ Kit; iNtRON Biotech Inc., Kyungki, Korea) according to the manufacturer's instructions. After imaging, the membranes were stripped and reprobed using anti-CREB and anti-beta-actin antibodies. The optical density (per mm^2) of each band was measured with a scanning laser densitometer (GS-700, Bio-Rad, Hercules, CA), and these values are presented as means± SEM. The ratios of the density of each p-CREB or p-ATF-1 band relative to that of the CREB or beta-actin band, respectively, were compared using Molecular Analyst software (Bio-Rad).

The data were analyzed using one-way ANOVA followed by the Student–Newman–Keuls post hoc test for multiple comparisons. In all cases, $p<0.05$ was taken as statistically significant.

4.6. Immunohistochemistry

Paraffin sections were used for the immunoperoxidase staining of p-CREB and rat macrophages, and frozen sections were used for the detection of T cells.

Briefly, paraffin-embedded spinal cords (5-μm sections) were deparaffinized by treatment with citrate buffer (0.01 M, pH 6.0) in a microwave for 10 min. To identify T cells, the frozen spinal cord sections were air-dried and fixed in 4% paraformaldehyde buffered with 0.1 M PBS (pH 7.2) for 20 min. After three washes with PBS, the sections were treated with 0.3% hydrogen peroxide in methyl alcohol for 20 min to block endogenous peroxidase activity.

After three washes with PBS, the sections were incubated with 10% normal goat or horse serum and then with the primary antigens, including rabbit polyclonal anti-p-CREB (1:200 dilution), ED1 (1:800 dilution), and R73 (1:1,000 dilution). Immunoreactivity was visualized using the avidin–biotin peroxidase reaction (Vector Elite kit, Vector, Burlingame, CA). Peroxidase was developed using a diaminobenzidine substrate kit (Vector). Sections were counterstained with hematoxylin before mounting. As a control, the primary antisera were omitted for a few test sections in each experiment.

To examine the cell phenotype in p-CREB expression, double immunofluorescence was applied using cell type-specific markers: ED1 for monocyte-like macrophages and anti-GFAP for astrocytes. First, paraffin sections were reacted sequentially with rabbit anti-p-CREB (1:100 dilution), biotinylated anti-rabbit IgG (Vector) (1:200 dilution), and tetramethyl rhodamine isothiocyanate (TRITC)-labeled streptavidin (Zymed, San Francisco, CA) (1:1,000 dilution). The slides were then incubated with ED1 (1:200 dilution) and anti-GFAP (1:200 dilution), followed by fluorescein isothiocyanate (FITC)-labeled goat anti-mouse IgG (1:50 dilution; Sigma).

To minimize lipofuscin autofluorescence, the sections were washed in PBS (3×1 h) at RT, dipped briefly in distilled H_2O, treated with 10 mM $CuSO_4$ in ammonium acetate buffer (50 mM CH_3COONH_4, pH 5.0) for 20 min, dipped briefly again in distilled H_2O, and then returned to PBS. The double immunofluorescence-stained specimens were examined under an FV500 laser confocal microscope (Olympus, Tokyo, Japan).

To semiquantify the immunostaining for p-CREB-positive neurons in the dorsal horn lamina, the number of p-CREB-positive dorsal horn neurons was counted in seven spinal cords from each group.

REFERENCES

Ahn, M., Moon, C., Lee, Y., Koh, C.S., Kohyama, K., Tanuma, N., Matsumoto, Y., Kim, H.M., Kim, S.R., Shin, T., 2004. Activation of extracellular signal-regulated kinases in the sciatic nerves of rats with experimental autoimmune neuritis. Neurosci. Lett. 372, 57–61.

Aicher, S.A., Silverman, M.B., Winkler, C.W., Bebo Jr., B.F., 2004. Hyperalgesia in an animal model of multiple sclerosis. Pain 110, 560–570.

Bender, R.A., Lauterborn, J.C., Gall, C.M., Cariaga, W., Baram, T.Z., 2001. Enhanced CREB phosphorylation in immature dentate gyrus granule cells precedes neurotrophin expression and indicates a specific role of CREB in granule cell differentiation. Eur. J. Neurosci. 13, 679–686.

Brindle, P.K., Montminy, M.R., 1992. The CREB family of transcription activators. Curr. Opin. Genet. Dev. 2, 199–204.

Buzas, B., Rosenberger, J., Kim, K.W., Cox, B.M., 2002. Inflammatory mediators increase the expression of nociceptin/orphanin FQ in rat astrocytes in culture. Glia 39, 237–246.

Caivano, M., Cohen, P., 2000. Role of mitogen-activated protein kinase cascades in mediating lipopolysaccharide-stimulated

induction of cyclooxygenase-2 and IL-1β in RAW264 macrophages. J. Immunol. 164, 3018–3025.

Crown, E.D., Ye, Z., Johnson, K.M., Xu, G.Y., McAdoo, D.J., Hulsebosch, C.E., 2006. Increases in the activated forms of ERK 1/2, p38 MAPK, and CREB are correlated with the expression of at-level mechanical allodynia following spinal cord injury. Exp. Neurol. 199, 397–407.

Etienne-Manneville, S., Chaverot, N., Strosberg, A.D., Couraud, P.O., 1999. ICAM-1-coupled signaling pathways in astrocytes converge to cyclic AMP response element-binding protein phosphorylation and TNF-alpha secretion. J. Immunol. 163, 668–674.

Johannessen, M., Delghandi, M.P., Moens, U., 2004. What turns CREB on? Cell Signal 16, 1211–1227.

Kingsley-Kallesen, M.L., Kelly, D., Rizzino, A., 1999. Transcriptional regulation of the transforming growth factor-beta2 promoter by cAMP-responsive element-binding protein (CREB) and activating transcription factor-1 (ATF-1) is modulated by protein kinases and the coactivators p300 and CREB-binding protein. J. Biol. Chem. 274, 34020–34028.

Liu, L., Wang, Y., Fan, Y., Li, C.L., Chang, Z.L., 2004. IFN-gamma activates cAMP/PKA/CREB signaling pathway in murine peritoneal macrophages. J. Interferon Cytokine Res. 24, 334–342.

Ma, W., Eisenach, J.C., 2002. Morphological and pharmacological evidence for the role of peripheral prostaglandins in the pathogenesis of neuropathic pain. Eur. J. Neurosci. 15, 1037–1047.

Ma, W., Quirion, R., 2001. Increased phosphorylation of cyclic AMP response element-binding protein (CREB) in the superficial dorsal horn neurons following partial sciatic nerve ligation. Pain 93, 295–301.

Mayr, B., Montminy, M., 2001. Transcriptional regulation by the phosphorylation-dependent factor CREB. Nat. Rev., Mol. Cell Biol. 2, 599–609.

Moon, C., Ahn, M., Kim, H., Lee, Y., Koh, C.S., Matsumoto, Y., Shin, T., 2005. Activation of p38 mitogen-activated protein kinase in the early and peak phases of autoimmune neuritis in rat sciatic nerves. Brain Res. 1040, 208–213.

Renno, T., Krakowski, M., Piccirillo, C., Lin, J.Y., Owens, T., 1995. TNF-alpha expression by resident microglia and infiltrating leukocytes in the central nervous system of mice with experimental allergic encephalomyelitis. Regulation by Th1 cytokines. J. Immunol. 154, 653–944.

Roach, S.K., Lee, S.B., Schorey, J.S., 2005. Differential activation of the transcription factor cyclic AMP response element binding protein (CREB) in macrophages following infection with pathogenic and nonpathogenic mycobacteria and role for CREB in tumor necrosis factor alpha production. Infect. Immun. 73, 514–522.

Rotshenker, S., 2003. Microglia and macrophage activation and the regulation of complement-receptor-3 (CR3/MAC-1)-mediated myelin phagocytosis in injury and disease. J. Mol. Neurosci. 21, 65–72.

Ryu, H., Lee, J., Impey, S., Ratan, R.R., Ferrante, R.J., 2005. Antioxidants modulate mitochondrial PKA and increase CREB binding to D-loop DNA of the mitochondrial genome in neurons. Proc. Natl. Acad. Sci. U. S. A. 102, 13915–13920.

Schonrock, L.M., Kuhlmann, T., Adler, S., Bitsch, A., Bruck, W., 1998. Identification of glial cell proliferation in early multiple sclerosis lesions. Neuropathol. Appl. Neurobiol. 24, 320–330.

Shin, T., Ahn, M., Jung, K., Heo, S., Kim, D., Jee, Y., Lim, Y.K., Yeo, E.J., 2003. Activation of mitogen-activated protein kinases in experimental autoimmune encephalomyelitis. J. Neuroimmunol. 140, 118–125.

Shin, T., Kojima, T., Tanuma, N., Ishihara, Y., Matsumoto, Y., 1995. The subarachnoid space as a site for precursor T cell proliferation and effector T cell selection in experimental autoimmune encephalomyelitis. J. Neuroimmunol. 56, 171–178.

Seger, R., Krebs, E.G., 1997. The MAPK signaling cascade. FASEB J. 9, 726–735.

Tanuma, N., Kojima, T., Shin, T., Aikawa, Y., Kohji, T., Ishihara, Y., Matsumoto, Y., 1997. Competitive PCR quantification of pro- and anti-inflammatory cytokine mRNA in the central nervous system during autoimmune encephalomyelitis. J. Neuroimmunol. 73, 197–206.

Velasco, S., Tarlow, M., Olsen, K., Shay, J.W., McCracken Jr., G.H., Nisen, P.D., 1991. Temperature-dependent modulation of lipopolysaccharide-induced interlukin-1 beta and tumor necrosis factor alpha expression in cultured human astroglial cells by dexamethasone and indomethacin. J. Clin. Invest. 87, 1674–1680.

Zaman, K., Ryu, H., Hall, D., O'Donovan, K., Lin, K.I., Miller, M.P., Marquis, J.C., Baraban, J.M., Semenza, G.L., Ratan, R.R., 1999. Protection from oxidative stress-induced apoptosis in cortical neuronal cultures by iron chelators is associated with enhanced DNA binding of hypoxia-inducible factor-1 and ATF-1/CREB and increased expression of glycolytic enzymes, p21(waf1/cip1), and erythropoietin. J. Neurosci. 19, 9821–9830.

ELSEVIER

Interferon beta-1b exacerbates multiple sclerosis with severe optic nerve and spinal cord demyelination ☆

Yoko Warabi [a,b,*], Yoh Matsumoto [b], Hideaki Hayashi [a]

[a] Department of Neurology, Tokyo Metropolitan Neurological Hospital, Tokyo, Japan
[b] Department of Molecular Neuropathology, Tokyo Metropolitan Institute for Neuroscience, Tokyo, Japan

Abstract

To evaluate the effect of interferon beta-1b (IFNB-1b) on multiple sclerosis (MS) with severe optic nerve and spinal cord demyelination, we examined the relationship between IFNB-1b treatment outcome and the clinical and genetic characteristics of three types of demyelinating diseases of the central nervous system, i.e., neuromyelitis optica (NMO), MS and MS with severe optic-spinal demyelination. Japanese MS frequently carried HLA DPB1*0501, which is associated with NMO. MS with DPB1*0501 showed severe optic-spinal demyelination represented by longitudinally extensive spinal cord lesion, blindness and CSF pleocytosis. IFNB-1b treatment did not succeed in these patients because of the increase of optic nerve and spinal cord relapse and other severe side effects. IFNB-1b should not be administered to demyelinating patients with genetic and clinical characteristics mimicking NMO such as HLA DPB1*0501 allele, longitudinally extensive spinal cord lesion, blindness and CSF pleocytosis even if they have symptomatic cerebral lesions as typically seen in MS. The present study strongly suggests that these patients should be diagnosed as having NMO.
© 2006 Elsevier B.V. All rights reserved.

Keywords: Neuromyelitis optica; Multiple sclerosis; Interferon beta-1b; Longitudinally extensive spinal cord lesion (LESL); Blindness; CSF pleocytosis

1. Introduction

Interferon beta-1b (IFNB-1b) treatment was reported to be effective for Japanese multiple sclerosis (MS) patients [1]. However, in Japan, there are a considerable number of MS patients with very severe optic nerve and spinal cord demyelination mimicking neuromyelitis optica [2,3]. Neuromyelitis optica (NMO) was defined as an inflammatory demyelinating disease in the central nervous system (CNS) in which the lesions are localized in the optic nerve and spinal cord [4]. Conversely, diagnostic criteria for MS only include patients who have cerebral lesions without a long spinal cord lesion extending over three vertebral segments and CSF pleocytosis [5]. Therefore,

patients with cerebral demyelinating lesions accompanied by longitudinally extensive spinal cord lesion and CSF pleocytosis were not classified as either NMO or MS, according to the previous diagnostic criteria. Recently, revised diagnostic criteria for NMO were published [6,7]. Autoantibodies called NMO-IgG taken from North American and Japanese NMO patients were reported to stain the perivascular and pial structures of the brain tissue [8,9], and the clinical characteristics of NMO-IgG-positive patients have been partially characterized [10]. However, appropriate treatment for such borderline patients remains difficult because the therapeutic strategy for NMO is different from that for MS.

In the present study, we hypothesized that IFNB-1b treatment is not effective for MS patients with severe optic nerve-spinal demyelination because these patients have genetic and clinical characteristics mimicking NMO. Based on this hypothesis, we retrospectively analyzed the clinical and genetic features of NMO, MS and borderline patients and examined the relationship between clinical and genetic phenotypes and the effects of IFNB-1b treatment. Consequently, we concluded

that IFNB-1b treatment rather exacerbated the clinical status of such borderline patients with cerebral demyelinating lesions accompanied by the NMO-specific HLA allele, DPB1*0501, longitudinally extensive spinal cord lesion, CSF pleocytosis and blindness.

2. Patients and methods

2.1. Patients

We evaluated a series of patients admitted to the Department of Neurology, Tokyo Metropolitan Neurological Hospital, Japan, between August and December 2003, and followed these patients until March 2006. At the time of admission, twenty-seven patients demonstrated clinically confirmed demyelinating disease in the CNS and had shown two or more separate attacks involving the cerebrum, spinal cord or optic nerve that were not attributable to other diseases. During the follow-up period, eight neurologists in our hospital examined each patient regularly and one of the study neurologists (YW) reviewed all medical records after the follow-up period.

2.2. Diagnosis

We diagnosed NMO ($n=12$) based on three "absolute criteria" from Wingerchuk's first diagnostic criteria that require optic neuritis, acute myelitis and an absence of evidence of clinical disease beyond the optic nerve or spinal cord [4]. The presence or absence of "supportive criteria" that include longitudinally extensive spinal cord lesion (LESL), CSF pleocytosis and severe optic neuritis is not considered for the diagnosis.

We diagnosed MS patients ($n=15$) according to McDonald's criteria. These patients had two or more demyelinating attacks including symptomatic cerebral lesions. Abnormality on "paraclinical tests" including LESL and CSF pleocytosis is not discussed for the diagnosis. We classified MS patients to one of the two clinical courses of MS: relapsing-remitting MS (RRMS) or secondary progressive MS (SPMS) after the follow-up period [11]. Eight patients had RRMS, seven had SPMS.

LESL was defined as hyperintensity over a length of three or more vertebral segments on T2-weighted sagittal images with a 1.5 T MRI scanner. CSF pleocytosis was defined as over 50 cells/μL. Severe optic neuritis was defined based on sequelae of bilateral or unilateral complete blindness. After the follow-up period, we reviewed all of the 27 patients' medical records and MRI images preserved in our hospital including those obtained before August 2003, and determined the presence or absence of these NMO-like characteristics in each patient.

2.3. Determination of the presence of HLA DPB1*0501 or DRB1*1501 alleles

Consent was obtained from all subjects tested and the study was approved by the Institute Review Board. Fifteen

milliliters of heparinized blood was drawn from 25 of 27 patients at the time of admission as well as from 36 healthy control subjects, then peripheral blood lymphocytes (PBL) were isolated using the density gradient method. RNA was extracted from PBL using RNAzol B (Biotecx Lab, Houston, TX) or TRIzol (Invitrogen, Tokyo, Japan). cDNA was synthesized using reverse transcription with ReverTra Ace-α (Toyobo, Osaka, Japan). The presence or absence of the DPB1*0501 or DRB1*1501 alleles in PBL samples was determined according to the protocol in the 13th International Histocompatibility Workshop. For the determination of DPB1*0501, cDNA was amplified using a DPB1-specific primer pair (5'-GAGAGTGGCGCCTCCGCTCAT-3' and 5'-GCCGGCCCAAAGCCCTCACTC-3'). Dot blot analysis was performed using the following five digoxigenin-labeled sequence-specific oligonucleotide (SSO) probes; DPB0901 (5'-GAATTACCTTTTCCAGGGA-3'), DPB5503 (5'-GGCCTGAGGCGGAGTACT-3'), DPB6906 (5'-GAGGAGAAGCGGGCAGTG-3'), DPB8503 (5'-AGCTGGACGAGGCCGTGA-3'), and DPB1701W (5'-GAATGCTACCCGTTTAAT-3'). The probes were labeled with digoxigenin using a DIG oligonucleotide tailing kit (Roche Applied Science, Mannheim, Germany). Detection of hybridized probes was conducted with the chemiluminescent signal detection system using CSPD (Tropix, Inc. Bedford, MA, USA).
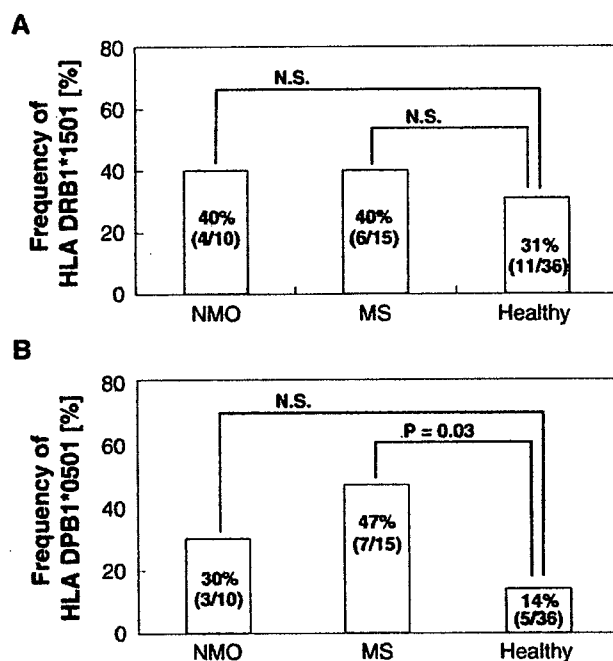
Fig. 1. HLA analysis in 10 NMO and 15 MS, and 36 healthy subjects. (A) Unexpectedly, the frequency of DRB1*1501 allele, which is known as a major HLA allele of MS patients, did not differ between our MS patients and healthy subjects, or between MS and NMO. N.S. indicated not significant. (B) DPB1*0501 allele, which has been reported to be associated with NMO, was carried significantly more frequently by the MS group than by healthy subjects ($p=0.03$).

For the determination of DRB1*1501, cDNA was amplified using a DR-2 specific primer pair (5′-TTCCTGT-GGCAGCCTAAGAGG-3′ and 5′-CCGCTGCACTGTG-GAGCTCT-3′). Then, the PCR products were examined for the DR2 allelic subtypes by dot blot analysis using four SSO. The SSO probes used in this study were as follows: DRB2813 (5′-GTTCCTGGACAGATACTT-3′), DRB7011 (5′-GACATCCTGGAGCAGGCG-3′), DRB8601 (5′-AAC-TACGGGGTTGGTGAG-3′), and DRB5706 (5′-GCCTGACGCTGAGTACTG-3′).

2.4. Interferon beta-1b (IFNB-1b) treatment

Eight million IU of IFNB-1b was injected subcutaneously every other day for 10 MS patients. Patients started this treatment either on admission to our hospital between August and December 2003 or before this admission. Five other MS patients were not treated with IFNB-1b because they refused treatment with this drug when their physicians provided information regarding the regimen. The treating physicians were blinded as to the HLA subtyping. Two NMO patients were also treated with IFNB-1b. However, their HLA were not analyzed because consent was not given by these two patients.

2.5. Statistical analysis

The frequencies of HLA DPB1*0501 and DRB1*1501 were analyzed using Fisher's exact probability method by a commercial software package (SPSS version 10.0J, SPSS Japan Inc, Tokyo, Japan).

3. Results

3.1. Japanese MS frequently carried HLA DPB1*0501 which is associated with NMO

We analyzed the frequency of HLA alleles in the MS and NMO groups (Fig. 1). Contrary to previous reports, the frequency of the DRB1*1501 allele, which is a major HLA allele of MS, did not differ between our MS and healthy subjects. Moreover, the DPB1*0501 allele, which is associated with NMO [12], was carried significantly more

Table 1
Clinical and genetic data of patients studied

Patient no.	Sex	Age, years	Clinical diagnosis	Disease duration, years	EDSS	DPB1*0501	DRB1*1501	Cerebral symptom	LESL	Blindness	CSF pleocytosis	Efficacy of IFNB-1b
1	M	50	RRMS	4	8.5	+	+	+	+	–	+	Relapse increased
2	F	45	RRMS	11	2.0	+	–	+	+	–	+	Relapse increased
3	F	54	RRMS	2	7.0	+	–	+	+	–	–	Skin ulcer
4	M	31	SPMS	8	7.5	+	+	+	–	+	–	Skin ulcer
5	F	52	SPMS	39	6.0	+	–	+	–	+	–	Relapse increased
6	M	26	RRMS	<1	2.0	+	–	+	–	–	–	Continued
7	M	47	SPMS	19	6.5	+	+	+	–	–	–	NA
8	M	37	SPMS	15	8.5	–	–	+	+	–	–	Continued
9	F	24	RRMS	<1	1.0	–	+	+	–	–	–	Continued
10	F	40	RRMS	4	2.0	–	–	+	–	–	–	Continued
11	M	33	RRMS	4	2.0	–	–	+	–	–	–	Continued
12	M	37	SPMS	11	6.0	–	+	+	–	–	–	NA
13	F	52	SPMS	8	7.0	–	+	+	–	–	–	NA
14	M	41	SPMS	26	7.5	–	–	+	–	–	–	NA
15	M	25	RRMS	<1	3.0	–	–	+	–	–	–	NA
16	F	77	NMO	2	7.5	+	–	–	+	+	–	NA
17	F	44	NMO	2	2.0	+	–	–	+	–	–	NA
18	F	36	NMO	9	7.0	+	+	–	–	–	–	NA
19	F	70	NMO	12	6.0	–	–	–	+	+	–	NA
20	F	62	NMO	9	2.0	–	–	–	+	–	+	NA
21	M	31	NMO	<1	6.0	–	–	–	+	–	–	NA
22	F	52	NMO	9	3.5	–	+	–	+	–	–	NA
23	F	57	NMO	16	1.0	–	+	–	+	–	–	NA
24	M	32	NMO	1	1.0	–	–	–	–	–	–	NA
25	F	41	NMO	22	2.0	–	+	–	–	–	–	NA
26	F	43	NMO	4	4.5	NT	NT	–	+	–	+	Skin ulcer
27	F	39	NMO	19	3.5	NT	NT	–	+	–	–	Skin ulcer

Disease duration=disease duration at entry to this study (August to December 2003).
LESL=longitudinally extensive spinal cord lesion.
IFNB-1b=interferon beta-1b.
NA=not administered.
Skin ulcer=patients who discontinued IFNB-1b due to skin ulcer.
Continued=patients who continued IFNB-1b because relapse did not markedly increase and there were no severe side effects.
NT=not tested.

Table 2
Positivity of severe optic-spinal characteristics and HLA allele, and effect of IFNB-1b in patients with MS and NMO

	"Supportive criteria" for NMO[a]	HLA				IFNB-1b treatment[b]
		DPB1*0501 (+) DRB1*1501 (−)	DPB1*0501 (+) DRB1*1501 (+)	DPB1*0501 (−) DRB1*1501 (+)	DPB1*0501 (−) DRB1*1501 (−)	
MS (n=15)	(+) (n=6)	3	2	0	1	Discontinued 5/6 (83%) Continued 1/6 (17%)
	(−) (n=9)	1	1	3	4	Discontinued 0/4 (0%) Continued 4/4 (100%)
NMO (n=10)	(+) (n=7)	2	0	2	3	NA
	(−) (n=3)	0	1	1	1	NA

[a] "Supportive criteria" for NMO include a longitudinally extensive spinal cord lesion, CSF pleocytosis and blindness.
[b] Cases/total administered (%).
IFNB-1b=interferon beta-1b.
NA=not administered.

frequently by MS patients (p=0.03) than by healthy subjects. Thus, our MS group was thought to consist of a heterogeneous population demonstrating genetic characteristics of both MS and NMO.

3.2. MS with DPB1*0501 showed severe optic neuritis, myelitis and CSF pleocytosis

We also analyzed the clinical characteristics of MS patients to determine whether some patients showed features of NMO. Of 7 patients of the MS group (n=15) who carried the DPB1*0501 allele, two patients (patients 1 and 2) showed both LESL and CSF pleocytosis (Table 1). One (patient 3) showed only LESL. Another two patients (patients 4 and 5) were blind. The remaining two (patients 6 and 7) did not show these manifestations of severe optic-spinal demyelination. In 8 MS patients without the DPB1*0501 allele, only one patient (patient 8) had LESL and none showed blindness or CSF pleocytosis. These findings demonstrate that MS patients with the DPB1*0501 allele, HLA associated with NMO, showed more severe optic neuritis, myelitis and CSF pleocytosis than MS patients without DPB1*0501.

3.3. IFNB-1b treatment was not successful in MS with genetic and clinical characteristics mimicking NMO

IFNB-1b treatment was discontinued in five MS patients for the following reasons (Table 1). Patient 1 developed a relapse with LESL after a few weeks of IFNB-1b administration and became confined to a wheelchair. IFNB-1b was discontinued for 6 months then restarted. Again, the patient developed another relapse with LESL. Patient 2 had experienced only three relapses during the past 9 years before IFNB-1b administration. Three months after IFNB-1b treatment, she developed two separate relapses in the cervical cord and optic nerve. Patient 5 showed secondary

progression of the disease without marked relapse for 7 years. Then, within 2 years after IFNB-1b treatment, she developed continuous progression and 5 episodes of marked relapses in the optic nerves leading to blindness. Patients 3 and 4 had severe skin ulcers at the injection sites requiring surgical repair. The other 5 patients continued IFNB-1b because relapse did not markedly increase and there were no severe side effects. Flu-like symptoms appeared in patients 6, 9 and 11, but disappeared within 3 months. There were no relapses during the follow-up period in patients 6, 9 and 10. One relapse in the cerebrum occurred in patient 11. Secondary progression did not markedly speed up and there was no marked relapse in patient 8. Thus, all five DPB1*0501-positive MS patients who met the "supportive criteria" for NMO, i.e., LESL, CSF pleocytosis or blindness, showed a poor prognosis following IFNB-1b treatment (Table 2). IFNB-1b treatment rather exacerbated the clinical status of patients with cerebral demyelinating lesions accompanied by LESL, CSF pleocytosis or blindness. These patients should be classified as having NMO even if they have symptomatic cerebral lesions.

IFNB-1b treatment was discontinued in two NMO patients because of the skin ulcers. Patient 26 had severe skin ulcers at the injection sites requiring surgical repair. Patient 27 developed small skin ulcers and keloids within 1 month of IFNB-1b treatment. Then, IFNB-1b was halted before the skin ulcers became more severe.

4. Discussion

In the present study, we found that there were two phenotypes in the patient group showing symptomatic cerebral demyelination. One phenotype is characterized by the presence of the NMO-specific HLA allele, DPB1*0501, and severe optic-spinal demyelination represented by longitudinally extensive spinal cord lesion, blindness and CSF

pleocytosis. Importantly, patients carrying this phenotype showed a poor prognosis following IFNB-1b treatment. In another phenotype, patients did not show severe optic nerve and spinal cord demyelination and were successfully treated with IFNB-1b. We demonstrated that IFNB-1b treatment increases the frequency of severe optic nerve and spinal cord relapses or skin ulcer as side effects in the former group of MS. IFNB-1b treatment was also discontinued in two of our NMO patients because skin ulcers developed as side effects. We suppose that severe skin ulcer at the injection sites requiring surgical repair is a side effect common to both NMO and MS with severe optic-spinal demyelination. IFNB-1b should not be administered to patients with genetic and clinical characteristics mimicking NMO such as the HLA DPB1*0501 allele, longitudinally extensive spinal cord lesion, blindness and CSF pleocytosis, even if they have symptomatic cerebral lesions as typically seen in MS.

Three NMO patients (patients 18, 24 and 25) did not fulfill any of the three "supportive criteria" for NMO (Table 2). They should have been diagnosed as having MS and treated with IFNB-1b even if they did not demonstrate typical cerebral demyelination. IFNB-1b treatment has been reported to be effective for the Japanese MS even in those with lesions localized in the optic nerve and spinal cord [1]. This group should be distinguished from NMO and rather included to MS according to the effect of IFNB-1b treatment.

We agree with the revised criteria for NMO [7]. We consider that the presence or absence of symptomatic cerebral lesions cannot be the absolute criterion for diagnosing NMO and that the presence of longitudinally extensive spinal cord lesion is essential for classification. The question is whether these criteria are also applicable to Japanese demyelinating patients. Nakashima et al. reported that the frequency of NMO-IgG in Japanese NMO was only 63%, although 15% of Japanese MS had NMO-IgG [10]. We suspect that the reason for the low frequency of NMO-IgG in NMO and the high frequency in MS might be misdiagnosis. As discussed above, there are two types of borderline patients in Japan. One phenotype is characterized by cerebral demyelinating lesions accompanied by NMO-specific HLA allele, DPB1*0501, and severe optic-spinal demyelination represented by longitudinally extensive spinal cord lesion, blindness and CSF pleocytosis. Another is MS with lesions localized in the optic nerve and spinal cord. We consider that the former phenotype is NMO and the latter is MS. Diagnosis and the frequency of NMO-IgG should be reanalyzed to these Japanese borderline patients. Conversely, they reported that complete blindness in at least one eye, as well as longitudinally extensive spinal cord lesion, was a significant feature in NMO-IgG-positive patients [10]. However, the revised criteria for NMO do not address the issues of blindness and CSF pleocytosis [7]. We should continue to discuss the diagnostic criteria for NMO using HLA subtyping and the old "supportive criteria" for NMO, i.e., longitudinally extensive spinal cord lesion, blindness and CSF pleocytosis.

One limitation of our study is that the limited number of patients was treated with IFNB-1b. In Japan, it has only been several years since IFNB-1b was approved for use to date and the number of patients treated with IFNB-1b remains limited. We should closely monitor a larger numbers of patients to obtain firmer conclusions.

In the present study, we analyzed the clinical and genetic features of NMO, MS and borderline patients and examined the relationship between clinical and genetic phenotypes and the effects of IFNB-1b treatment. The outcomes demonstrated that IFNB-1b should not be administered to demyelinating patients with genetic and clinical characteristics mimicking NMO such as HLA DPB1*0501 allele, longitudinally extensive spinal cord lesion, blindness and CSF pleocytosis even if they demonstrate symptomatic cerebral lesions. These patients should be classified as having NMO even if they have symptomatic cerebral lesions.

References

[1] Saida T, Tashiro K, Itoyama Y, Sato T, Ohashi Y, Zhao Z. Interferon beta-1b is effective in Japanese RRMS patients: a randomized, multicenter study. Neurology 2005;64(4):621–30.

[2] Fukazawa T, Kikuchi S, Niino M, Yabe I, Miyagishi R, Fukaura H, et al. Attack-related severity: a key factor in understanding the spectrum of idiopathic inflammatory demyelinating disorders. J Neurol Sci 2004;225(1–2):71–8.

[3] Fukazawa T, Kikuchi S, Miyagishi R, Miyazaki Y, Fukaura H, Yabe I, et al. CSF pleocytosis and expansion of spinal lesions in Japanese multiple sclerosis with special reference to the new diagnostic criteria. J Neurol 2005;252(7):824–9.

[4] Wingerchuk DM, Hogancamp WF, O'Brien PC, Weinshenker BG. The clinical course of neuromyelitis optica (Devic's syndrome). Neurology 1999;53(5):1107–14.

[5] McDonald WI, Compston A, Edan G, Goodkin D, Hartung HP, Lublin FD, et al. Recommended diagnostic criteria for multiple sclerosis: guidelines from the International Panel on the Diagnosis of Multiple Sclerosis. Ann Neurol 2001;50(1):121–7.

[6] Pittock SJ, Lennon VA, Krecke K, Wingerchuk DM, Lucchinetti CF, Weinshenker BG. Brain abnormalities in neuromyelitis optica. Arch Neurol 2006;63(3):390–6.

[7] Wingerchuk DM, Lennon VA, Pittock SJ, Lucchinetti CF, Weinshenker BG. Revised diagnostic criteria for neuromyelitis optica. Neurology 2006;66(10):1485–9.

[8] Lennon VA, Wingerchuk DM, Kryzer TJ, Pittock SJ, Lucchinetti CF, Fujihara K, et al. A serum autoantibody marker of neuromyelitis optica: distinction from multiple sclerosis. Lancet 2004;364(9451):2106–12.

[9] Lennon VA, Kryzer TJ, Pittock SJ, Verkman AS, Hinson SR. IgG marker of optic–spinal multiple sclerosis binds to the aquaporin-4 water channel. J Exp Med 2005;202(4):473–7.

[10] Nakashima I, Fujihara K, Miyazawa I, Misu T, Narikawa K, Nakamura M, et al. Clinical and MRI features of Japanese MS patients with NMO-IgG. J Neurol Neurosurg Psychiatry 2006;77(9):1073–5.

[11] Lublin FD, Reingold SC. Defining the clinical course of multiple sclerosis: results of an international survey. National Multiple Sclerosis Society (USA) Advisory Committee on Clinical Trials of New Agents in Multiple Sclerosis. Neurology 1996;46(4):907–11.

[12] Yamasaki K, Horiuchi I, Minohara M, Kawano Y, Ohyagi Y, Yamada T, et al. HLA-DPB1*0501-associated opticospinal multiple sclerosis: clinical, neuroimaging and immunogenetic studies. Brain 1999;122 (Pt 9):1689–96.

Nonviral Aβ DNA vaccine therapy against Alzheimer's disease: Long-term effects and safety

Yoshio Okura*, Akira Miyakoshi*, Kuniko Kohyama*, Il-Kwon Park*, Matthias Staufenbiel†, and Yoh Matsumoto*†

*Department of Molecular Neuropathology, Tokyo Metropolitan Institute for Neuroscience, Musashidai 2-6, Fuchu, Tokyo 183-8526, Japan; and †Neuroscience Research, Novartis Institutes of Biomedical Research, CH-4002 Basel, Switzerland

It was recently demonstrated that amyloid β (Aβ) peptide vaccination was effective in reducing the Aβ burden in Alzheimer model mice. However, the clinical trial was halted because of the development of meningoencephalitis in some patients. To overcome this problem, anti-Aβ antibody therapy and other types of vaccination are now in trial. In this study, we have developed safe and effective nonviral Aβ DNA vaccines against Alzheimer's disease. We administered these vaccines to model (APP23) mice and evaluated Aβ burden reduction. Prophylactic treatments started before Aβ deposition reduced Aβ burden to 15.5% and 38.5% of that found in untreated mice at 7 and 18 months of age, respectively. Therapeutic treatment started after Aβ deposition reduced Aβ burden to≈50% at the age of 18 months. Importantly, this therapy induced neither neuroinflammation nor T cell responses to Aβ peptide in both APP23 and wild-type B6 mice, even after long-term vaccination. Although it is reported that other anti-Aβ therapies have pharmacological and/or technical difficulties, nonviral DNA vaccines are highly secure and easily controllable and are promising for the treatment of Alzheimer's disease.

amyloid β-peptide | DNA vaccination

A lzheimer's disease is a chronic neurodegenerative disorder that is the most common cause of progressive impairment of memory and cognitive function in aged humans. The etiology of the disease is thought to be the result of an imbalance between amyloid β (Aβ) production and clearance (amyloid cascade hypothesis) (1, 2). On the basis of this hypothesis, Schenk et al. (3) developed an Aβ-peptide vaccine, immunized amyloid precursor protein (APP)-transgenic mice with the peptide in complete Freund's adjuvant (CFA), and demonstrated a marked amyloid reduction in the brain. Repetitive intranasal administration of Aβ-peptide and adjuvant (4) and the passive transfer of anti-Aβ antibodies were also effective in reducing amyloid deposits (5). Moreover, vaccinated mice showed an improvement in memory loss (6, 7). Thus, Aβ peptide vaccine therapy has been shown to be effective in animal models, and human clinical trials were started with Betabloc (AN-1792), composed of synthetic Aβ1-42 and QS21 as an adjuvant (8). However, the phase II clinical trial was halted because of the development of acute meningoencephalitis that appeared in 18 (6%) of 298 vaccinated patients (9). Importantly, it was later demonstrated by autopsy that there was a significant reduction of amyloid deposition and disappearance of degenerative axons in a treated patient (10). At the same time, T cell-dominant meningeal encephalitis was present in the cerebral cortex. These findings suggest that the vaccine therapy is a promising strategy for human Alzheimer's disease if excessive immune reactions are minimized to avoid unwanted neuroinflammation.

Recently, it was reported that naked plasmid DNAs encoding proteins are taken into cells and produce the proteins in a small amount for a relatively long period when injected into the muscle or skin (11). Then, the proteins that are released in the extracellular space induce antibodies against the proteins (12, 13). Thus, gentle and quiet immune reactions could be obtained by DNA vaccine administration. In our and other's laboratories,

immune therapies with DNA vaccines have been examined in autoimmune disease models (14–17) and have been found to be effective in preventing the diseases without the use of adjuvants. Here, we developed nonviral Aβ DNA vaccines and were able to reduce the amyloid burden in the cerebral cortex and hippocampus of Alzheimer's disease model (APP23) mice by vaccination. Importantly, the side effects, such as T cell proliferation and neuroinflammation, were absent even after long-term administration of the vaccines in both APP23 and wild-type B6 mice.

Results

Preparation and Characterization of Nonviral Aβ DNA Vaccines. We prepared three types of nonviral Aβ DNA vaccines using a mammalian expression vector, pTarget. The sequence of Aβ1-42 and additional sequences were inserted in the plasmid, as shown in Fig. 1A. The first one contains only the Aβ1-42 sequence with the Kozak sequence at the 5′ end (referred to as K-Aβ vaccine) (Fig. 1A1). To the second, the Igκ signal sequence of mouse Ig was added to improve the secretion ability (IgL-Aβ vaccine) (Fig. 1A2), and the third possesses the Fc portion of human Ig at the 3′ end to maintain stability (Aβ-Fc vaccine) (Fig. 1A3). Before in vivo administration, these DNA vaccines were transfected to HEK295T cells, and the secretion of Aβ1-42 peptide into the culture supernatant was assayed with Western blotting (Fig. 1B). The production of intracellular Aβ1-42 peptide was confirmed in all three vaccines by ELISA (data not shown). It was clearly demonstrated that the supernatants of cultured cells that had been transfected with IgL-Aβ and Aβ-Fc vaccines contained translated proteins (4.5 and 35 kDa, respectively), whereas K-Aβ-transfected cells did not secrete the peptide into the extracellular space. These findings indicate that the addition of the leader sequence is important for transportation of the protein to the extracellular space as reported in ref. 18 and that this event is critical for the effects of DNA vaccines (see below).

Reduction of Amyloid Burden by Aβ DNA Vaccination. We used two types of regimens to examine the effect of Aβ DNA vaccination, i.e., prophylactic and therapeutic. For the prophylactic protocol, vaccine administration was started at 3–4 months of age, before the appearance of amyloid deposition. APP23 mice received 6 weekly and subsequent biweekly injections of the vaccines and were examined at 7, 9, 12, 15, and 18 months of age (Fig. 1C1). The paraffin-embedded sections of the brain were stained immunohistochemically with 6F/3D against Aβ8-17, and the area of amyloid depositions was quantitated as the total sum of the pixels with NIH IMAGE software.

IMMUNOLOGY

A

1) pTarget-Aβ (Aβ)

Kozak

| A beta 1-42 |

pTarget

2) pTarget-Ig-Aβ (IgL)

| Ig leader | A beta 1-42 |

pTarget

3) pTarget-Ig-Aβ-Fc (Fc)

| Ig leader | A beta 1-42 | human IgFc |

pTarget

B

← 35 kDa

← 4.5 kDa

C

1) Prophylactic administration

Amyloid plaque

3 m 6 m 7 m 9 m 12 m 15 m 18 m

S-1 S-2 S-3 S-4 S-5

Weekly x 6   Biweekly

2) Therapeutic administration
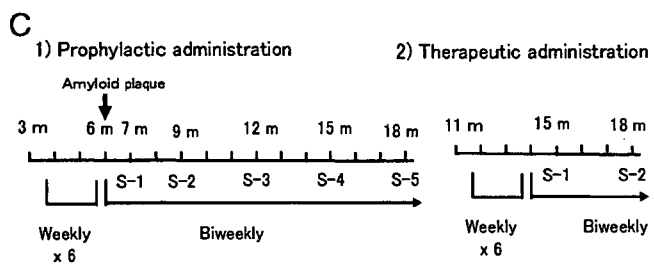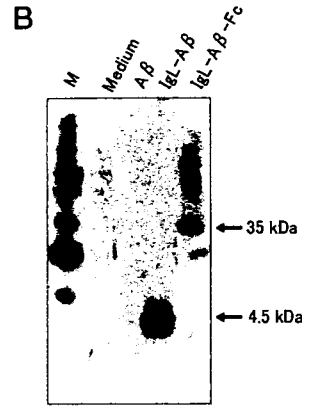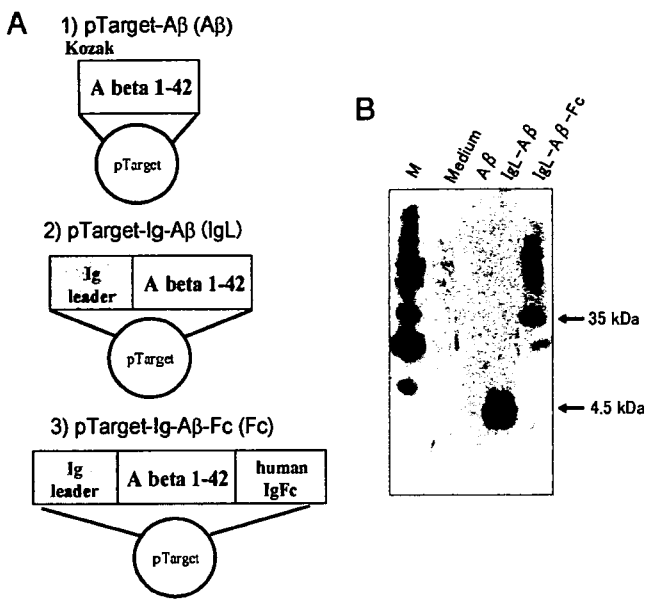
11 m 15 m 18 m

S-1 S-2

Weekly x 6   Biweekly

Fig. 1. Construction of DNA vaccines (A), in vitro characterization (B) and the treatment protocol (C). (A) Three DNA vaccines were produced by using a mammalian expression vector. DNA encoding the Aβ1-42 sequence was inserted in XhoI/KpnI site of the plasmid (K-Aβ vaccine) (A1). In the second vaccine, the signal sequence of mouse Igκ is added to the 5′ end to improve the secretive efficiency (IgL-Aβ vaccine) (A2). The third vaccine possesses the Fc portion of human immunoglobulins to improve the stability of the secreted protein (Aβ-Fc vaccine) (A3). (B) Western blot analysis revealed that translated Aβ proteins were detected in supernatants of cultured cells transfected with IgL-Aβ and Aβ-Fc vaccines. (C) The protocol of vaccine treatment. To examine the prophylactic effect of DNA vaccines, the vaccines were administrated to APP23 mice starting from 3–4 months of age, before the appearance of amyloid depositions. The mixture of one of the vaccines (100 μg) and bupivacaine (0.25 mg) was injected intramuscularly on a weekly basis for the first 6 weeks. Then, the vaccine without bupivacaine was injected every 2 weeks thereafter. Mice were sampled at 7, 9, 12, 15, and 18 months of age (C1). For therapeutic treatment, the vaccines were administered to APP23 mice starting from 12 months of age, after the appearance of amyloid plaques. Samplings were performed at 15 and 18 months of age (C2). m, months of age.

In the first series of the prophylactic treatment, mice were analyzed at 7, 9, and 12 months of age (Table 1, Exp. 1). At 7 months of age, granular amyloid depositions were recognized in the frontal cortex in the control groups (empty-vector-administered and untreated mice) (Fig. 2B). At this stage, Aβ plaques were not detected in the hippocampus (data not shown). In sharp contrast, cortical Aβ depositions in mice treated with Aβ-Fc (Fig. 2A), IgL-Aβ, and Aβ (data not shown) vaccines were significantly reduced (P < 0.01). The Aβ burden was reduced to ≈15–30% of the untreated groups (Fig. 2E). At 12 months of age, amyloid depositions in untreated mice were increased, and some of them became large (>50 μg) in the frontal cortices of the untreated mice (Fig. 4C, which is published as supporting information on the PNAS web site). Cortical

Table 1. Summary of experimental data on nonviral Aβ DNA vaccine therapy against Alzheimer model mice

Exp.	Group	Strain	No. of animals	Start of Tx, mo	Sampling, mo	Duration of Tx, mo	Regimen	Weekly	Biweekly	Monthly	% Aβ burden (cortex) Fc	IgL	K-Aβ	Emp	No Tx	% Aβ burden (hippocampus) Fc	IgL	K-Aβ	Emp	No Tx	CD5	Mac3
1	1	Tg	15	4	7	3	Prophylactic	×6	×3		15.5	18.2	31.4	93.1	100	N.T.	N.T.	N.T.	N.T.	N.T.	Neg	Neg
	2	Tg	32	4	9	5	Prophylactic	×6	×8		12.7	13.3	28.1	103	100	N.T.	N.T.	N.T.	N.T.	N.T.	Neg	Neg
	3	Tg	17	4	12	8	Prophylactic	×6	×12		33.7	28.6	51.3	103	100	22	26	65.3	114	100	Neg	Neg
2	1	Tg	20	3	15	12	Prophylactic	×6	×24		30.6	37.2	N.T.	91.2	100	32.5	38.4	N.T.	96	100	Neg	Neg
	2	Tg	16	3	18	15	Prophylactic	×6	×29		38.5	46.2	N.T.	91.3	100	36.4	44.8	N.T.	99.5	100	Neg	Neg
3	1	Tg	23	12	15	3	Therapeutic	×6	×4		42.4	41.6	N.T.	98.1	100	40.3	43.5	N.T.	100	100	Neg	Neg
	2	Tg	19	12	18	6	Therapeutic	×6	×10		47	49.9	N.T.	96.7	100	38	46	N.T.	86.6	100	Neg	Neg
4	1	Tg	18	7	15	8	Therapeutic			×9	67.6	81.7	N.T.	90.6	100	69.4	73.9	N.T.	95.6	100	Neg	Neg
	2	Tg	16	7	18	11	Therapeutic			×12	79.6	88.1	N.T.	91.7	100	74.8	75.6	N.T.	92	100	Neg	Neg
5	1	B6	25	4	7	3	—	×6	×4		N.T.	N.T.	N.T.	N.T.	N.T.	N.T.	N.T.	N.T.	N.T.	N.T.	Neg	Neg
	2	B6	25	4	9	5	—	×6	×9		N.T.	N.T.	N.T.	N.T.	N.T.	N.T.	N.T.	N.T.	N.T.	N.T.	Neg	Neg
	3	B6	24	4	12	8	—	×6	×14		N.T.	N.T.	N.T.	N.T.	N.T.	N.T.	N.T.	N.T.	N.T.	N.T.	Neg	Neg

The vaccines were administered for the indicated duration to a large number of mice (176 APP23 and 74 B6 mice). In Exp. 1, the mice were divided into five groups as follows: Aβ-Fc vaccine administration, IgL-Aβ vaccine administration, K-Aβ vaccine administration, empty-vector administration, and no treatment. In Exps. 2–5, the K-Aβ vaccine administration group was excluded from the analysis because of its lower efficacy than other two vaccines. Each group consisted of 4–6 mice. Prophylactic effects were examined in Exps. 1 and 2. Therapeutic effects were examined in Exps. 3 and 4. All APP23 mice were analyzed immunohistochemically with mAb (6F/3D) against Aβ7-18. Then, the reduction of amyloid plaque was quantified, as shown in Materials and Methods. In Exp. 5, DNA vaccines were administered to B6 mice to know whether the vaccines induce neuroinflammation. Tissues from three mice in each group were immunohistochemically stained with mAbs against CD5 and Mac-3. Neg, negative finding, i.e., no neuroinflammation; N.T., not tested; Exp., experiment; Tx, treatment; Tg, transgenic; Emp, empty vector.
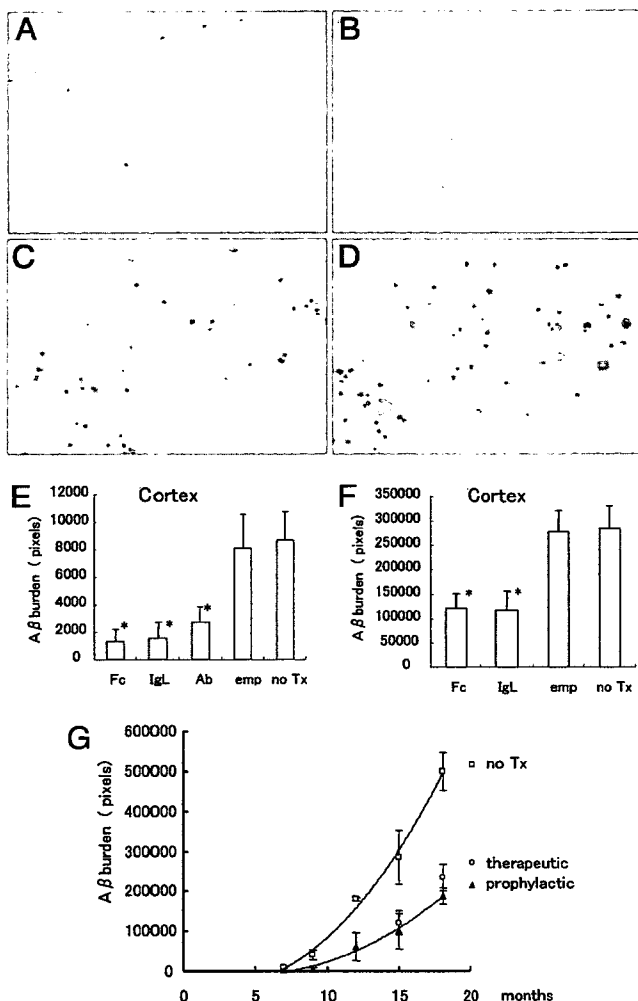
Fig. 2. Reduction of Aβ burden in APP23 mice after DNA vaccination. (A) In mice vaccinated with Aβ-Fc vaccine, amyloid plaques in the frontal cortex were reduced after 3 months of prophylactic treatment. (B) Immunohistochemical examinations revealed that granular amyloid depositions were detected in the frontal cortices of untreated mice at 7 months of age. (C) Amyloid plaques were reduced in mice treated with Aβ-IgL vaccine. (D) At 15 months of age amyloid plaques of variable size were detected in the frontal cortices of untreated mice. (E) Quantitative analysis demonstrated that the cortical Aβ burden at 7 months was significantly decreased (P < 0.01) after the prophylactic treatment with Aβ-Fc (15.5% of untreated controls), IgL-Aβ (18.2%), and Aβ vaccine (31.4%) compared with those found in untreated and empty-vector-vaccinated mice. (F) Therapeutic treatment with Aβ-Fc and IgL-Aβ vaccines significantly reduced (P < 0.01) cortical Aβ burden at 15 months. The overall quantitative analysis is depicted in G. The amyloid deposition was first detected in untreated mice at 7 months of age and rapidly increased after 15 months of age (open squares). Prophylactic administration of Fc-Aβ vaccine prevented the Aβ deposition to 10–30% of that in untreated animals before 12 months of age and to 40–50% after 15 months (filled triangles). The effects of therapeutic administration were almost the same as those of prophylactic administration (open circles). Tx, treatment; emp, empty vector. Original magnification, ×62 (A and B); ×24 (C and D).

Aβ depositions were significantly reduced (P < 0.01) to ≈30–50% of the untreated group (Fig. 4D) after Aβ-Fc (Fig. 4A) and IgL-Aβ (Fig. 4B) vaccine treatment. Aβ depositions in the hippocampus were also decreased equally (P < 0.01) (Table 1, Exp. 1, Group 3). It was shown that the suppressive effect of Aβ-Fc vaccine was almost equal to IgL-Aβ vaccine. However, K-Aβ vaccine was less effective than the former two (Figs. 2E and 4D) and was not used in subsequent experiments. The

second part of the prophylactic treatment analyzed the mice at 15 and 18 months of age (Table 1, Exp. 2). At these time points, the plaques in untreated groups had rapidly increased. Untreated APP23 mice showed an age-dependent increase of amyloid plaques in the cerebral cortex (Fig. 2G, open squares) and hippocampus (data not shown). The prophylactic protocol, using Aβ-Fc vaccine, revealed that the final reduction rate of Aβ burden in the cerebral cortex at 18 months of age was ≈38.5% of untreated groups (Table 1, Exp. 2 and Fig. 2G, closed triangles). These results demonstrated that two of the three vaccines produced in this study were effective in prophylactic treatment.

When considering the clinical applications, it is critical to know the effects of the vaccines in therapeutic application. For this purpose, the vaccination was started at 12 months of age, 6 months after the start of Aβ deposition, and the brains were examined at 15 (Fig. 2) and 18 (Fig. 5, which is published as supporting information on the PNAS web site) months of age. In therapeutic treatment, amyloid plaques in the cortex were significantly decreased (P < 0.01) (Fig. 2F) by Aβ-Fc and IgL-Aβ vaccination (Fig. 2D) compared with the controls (Fig. 2C). Aβ depositions in the hippocampus were also decreased (P < 0.01) (Table 1, Exp. 3). Although the therapeutic protocol (Fig. 2G, open circles) seemed to be less effective than the prophylactic one (Fig. 2G closed triangles), the difference was not significant. It should be noted that APP23 mice treated with the therapeutic protocol received DNA vaccines for only 3 and 6 months, respectively (Table 1, Exp. 3). Thus, Aβ DNA vaccines had sufficient effects, even if the vaccines were administrated after amyloid depositions appeared.

Recently, it was reported that the intracellular Aβ deposition in cortical pyramidal neurons is the first neurodegenerative event in Alzheimer's disease development (19). Therefore, we counted the number of neurons containing intracellular Aβ depositions in the cortices of Aβ-Fc-vaccine-administered and control mice. Aβ-deposited neurons were significantly decreased with both the prophylactic (50.2% of untreated control, P < 0.01) and therapeutic (59.54%, P < 0.05) treatments at 15 months of age (Fig. 6, which is published as supporting information on the PNAS web site).

Change in the Serum Aβ Antibody Titer After Vaccine Administration.
The titers of serum anti-Aβ antibodies after the prophylactic treatment (Table 1, Exps. 1 and 2) were determined by ELISA. The levels of anti-Aβ antibodies were significantly increased (**, P < 0.01; *, P < 0.05) 2- to 4-fold compared with the untreated and empty-vector-vaccinated mice (Fig. 3A). The titers showed an age-dependent increase in both treated and untreated mice, because the antibody production was induced in untreated APP23 mice by high levels of Aβ in the sera of aged mice. In contrast, the anti-Aβ antibodies in the sera of wild-type B6 mice were below the detection limit (data not shown). We also analyzed the relationships between the amounts of amyloid depositions and anti-Aβ titers (Fig. 3B). The amounts of amyloid depositions were significantly smaller in mice with high antibody titers. A significant correlation between the antibody titer and the reduction of Aβ burden was observed at 7 months (r = −0.642) (Fig. 3B, 7 months) and 9 months (r = −0.38965) (Fig. 3B, 9 months) of age by the CORREL function. The difference became less clear at a later stage (Fig. 3B, 12 months).

T Cell-Proliferation Assay After Vaccine Administration. To determine whether DNA vaccination induces the T cell activation and proliferation that are key steps for the development of neuroinflammation, APP23 and B6 mice were injected with DNA vaccines. A group of mice were also immunized with Aβ peptide/CFA. Three weeks after the first injection, lymphocytes were isolated and cultured with Aβ peptide (0–10 μM) for 3
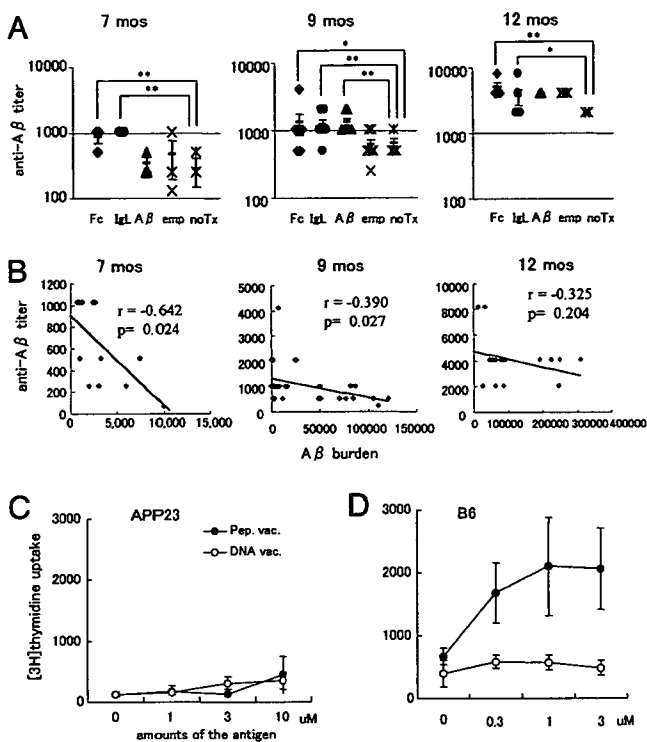
Fig. 3. B and T cell responses of mice treated with Aβ DNA vaccines. (A and B) Titration of anti-Aβ antibodies in vaccinated APP23 mice. The anti-Aβ antibody titer in treated mice was significantly increased (∗∗, $P < 0.01$; ∗, $P < 0.05$) ≈2- to 4-fold compared with the untreated group. The titer levels were increased in untreated APP23 as well as treated mice at the same age period (A). There was significant correlation between the serum anti-Aβ antibody titer and the reduction of amyloid depositions at 7 months of age (CORREL function $r = -0.642$, $t0 = 2.648 > t10 = 2.228$) (B). At 9 months of age, a significant correlation was present, but the difference was less marked compared with that at 7 months ($r = -0.38965$, $t0 = 3.10 > t22 = 2.086$). A significant difference was not noted at 12 months of age ($r = -0.325$, $t0 = 1.3309 < t17 = 2.110$). (C and D) T cell responses in APP23 (C) and B6 (D) mice after immunization with Aβ peptide/CFA or DNA vaccination. Lymphocytes isolated from two strains were incubated with Aβ peptide (0–10 μM) for 3 days. Incorporation of [³H]thymidine was measured by liquid scintillation spectrometry. In APP23 mice, neither T cells from peptide-immunized mice nor those from DNA-vaccinated mice were activated in the presence of Aβ1-42 (C). In contrast, Aβ peptide immunization, but not DNA vaccination, induced a significant T cell response in B6 mice (D). All of the data are the mean values ± SD, and the representative results from three different experiments are shown. Tx, treatment; emp, empty vector.

days. Incorporation of [³H]thymidine was measured by using liquid scintillation spectrometry. T cells from APP23 mice did not react with Aβ peptide after both Aβ DNA vaccine and Aβ peptide administration (Fig. 3C). In sharp contrast, T cells from B6 mice responded significantly to Aβ peptide after immunization with Aβ peptide, but not after Aβ DNA vaccination (Fig. 3D). Notably, Aβ DNA vaccination did not induce T cell proliferation in either APP or B6 mice after three injections (Fig. 3C) and 5-month treatment (data not shown). These findings suggest that T helper (Th)1 cells in APP23 mice are in an immunologically tolerant state against Aβ1-42, probably because of long-term exposure to a high level of Aβ1-42.

Pathological Examination of the Brains of Vaccinated Mice. The presence or absence of neuroinflammation in the brain was examined immunohistochemically after the long-term administration of DNA vaccines. Because the T cell assay demonstrated the significant differences between APP23 and B6 mice, patho-

logical examinations were performed in both strains. Brain sections were stained with anti-CD5 mAb against T cells and with Mac-3 against macrophages. In the thymus (Fig. 7A, which is published as supporting information on the PNAS web site) and spleen (Fig. 7B), a large number of lymphocytes and macrophages were stained positively. In sharp contrast, inflammatory foci in the brain parenchyma and meninges were not detected in either APP23 (Fig. 7 C and D) or B6 (Fig. 7 E and F) mice.

Discussion

In this study, we developed nonviral Aβ DNA vaccines against Alzheimer's disease and demonstrated satisfactory effects in the Aβ reduction in model mice. With the prophylactic and therapeutic protocols, treatment with both IgL-Aβ and Aβ-Fc reduced Aβ burden in the cerebral cortex to ≈40–50% of the untreated controls, although the latter was slightly more effective than the former. It should be noted that mice killed at 18 months of age received DNA vaccines for only the last 6 months. These findings suggest that relatively short-term vaccination is sufficient for the reduction of Aβ burden. Because it was demonstrated in the other experimental setting that 50% reduction of Aβ burden resulted in full recovery of the cognitive disturbance (6), the suppressive effects of DNA vaccines demonstrated in this study is satisfactory. Furthermore, it was reported that Aβ immunotherapy reduces not only extracellular Aβ plaques but also intracellular Aβ accumulation and, most notably, leads to the clearance of early tau pathology by using the triple-transgenic model of Alzheimer's disease (20–22). Taken together, the outcome of DNA vaccine therapy is promising when applied to human Alzheimer's disease.

The elevation of anti-Aβ antibodies was also detected after DNA vaccination. However, the antibody elevation was mild to moderate (≈2- to 4-fold) compared with that found in mice that had received Aβ peptide (10,000-fold) (3). The adjuvant in peptide vaccines (23) may activate Th1 type T cells (10), which induce the rapid increase of antibody titers as a result. As demonstrated in this study, DNA vaccination was able to be performed without adjuvants, resulting in the absence of obvious T cell proliferation in both APP23 and B6 mice (Fig. 7) and did not cause neuroinflammation, even after long-term DNA vaccination (Fig. 7, which is published as supporting information on the PNAS web site). Importantly, mild elevation of the antibody titers induced by DNA vaccines could reduce amyloid deposits, probably because DNA vaccination constantly induces the antibody production at a low titer for a long period. Thus, the maintenance of high anti-Aβ antibody titer levels is not necessary for effective treatment with DNA vaccines.

To minimize excessive immune reaction in mice and patients, we should recognize the difference in immunological reactions against Aβ between the Alzheimer model and wild-type mice. As clearly demonstrated here, there was no Th1 cell response to Aβ peptide in APP23 mice after Aβ peptide/CFA injection, whereas, in B6 mice, the same immunization protocol induced a significant T cell response against Aβ peptide (Fig. 3D). These findings strongly suggest that autoreactive Th1 cells in model mice are in a state of immune tolerance because of a high Aβ expression from an early stage of life. In contrast, Th2 cells helping the antibody production seem to be working, as evidenced by the fact that vaccinated animals possessed elevated levels of anti-Aβ antibodies. Similar findings were reported by Qu et al. (24), with gene-gun administration of Aβ plasmid DNA. Monsonego et al. (25) also reported that the immune responses of T and B cells of model mice are low compared with those of wild-type mice. In contrast, a significant T cell reactivity to Aβ peptide was detected in patients with Alzheimer's disease (23). Thus, strong immune induction is dangerous for patients with Alzheimer's disease.

The CpG motif, which exists in plasmid DNAs, is reported to induce Th1-type immunity and up-regulates IFN-γ production under certain circumstances (26–28). However, this phenomenon is observed only when a relatively high dose of CpG oligonucleotides is used (29). In contrast, empty vectors containing the CpG motif ameliorated the clinical and histological severity of the autoimmune encephalomyelitis that is thought to be a Th1-mediated disease, as shown in previous studies by us (30) and others (31, 32).

Recently, Aβ DNA vaccines were developed by using virus vectors (33, 34). Although, these vaccines effectively decreased Aβ depositions in the brains of model mice, the possibility of viral replication could not be completely excluded. The plasmid vector is safe and has no possibility of viral infection and transformation because it exists as an episome without being built into the chromosome in eukaryotic cells (12, 13). Another important factor is related to technology. When DNA vaccines are in clinical use, large amounts of vaccines are necessary for treatment of a large number of patients who would be treated for a long period. Nonviral DNA vaccines have an advantage because they can be mass-produced with a high purity at a low price.

In summary, we demonstrated that nonviral Aβ DNA vaccines are highly effective and safe in reducing the Aβ burden in model mice and, thus, are promising as a vaccine therapy against human Alzheimer's disease.

Materials and Methods

Animals. The APP23 transgenic mice used in this study express human APP751 cDNA with Swedish double mutation under the control of the neuron-specific mouse Thy-1 promoter (35, 36). The Thy-1 expression cassette lacks intron 3, which contains the elements required for expression in the thymus. RT-PCR and Western blot analysis of APP23 mice have confirmed the lack of detectable expression of the transgene in the thymus and spleen (D. Abramowski, C. Sturchler-Pierrat, and M.S., unpublished data). This finding is in agreement with a report by Moechars *et al.* (37), who used the same expression cassette and also found that the exogenous transgene with this promoter sequence is expressed only in the brain but not in the thymus. APP23 mice were initially established on a B6D2 background and have been continuously backcrossed to C57BL/6J (B6). In APP23 mice, amyloid depositions appear from 6 months of age, predominantly in the neocortex and hippocampus. Aβ plaques have most of the characteristics of human Alzheimer's disease plaques, including fibrillary Aβ cores, and are surrounded by dystrophic neuritis and activated glial cells. Region-specific amyloid-associated neurodegeneration, including neuron loss, synapse deficits, and cholinergic alterations, are present in these mice (38). Wild-type B6 mice were purchased from Charles River Breeding Laboratories (Kanagawa, Japan). All animal experiments were approved by the institute committee and performed in accordance with institutional guidelines.

The Development of DNA Vaccine. We prepared three Aβ DNA vaccines using a pTarget mammalian expression system (Promega, Tokyo) (Fig. 1*A*). The DNA fragment, encoding Aβ1-42, was made to anneal two oligonucleotides covering the entire Aβ1-42 sequence. The Kozak sequence was inserted at the 5' end of the Aβ1-42 sequence (referred to as K-Aβ vaccine). In the second vaccine, the signal sequence of mouse Igκ was added to the 5' end of the Aβ1-42 sequence to improve the secretory efficiency of Aβ peptide (IgL-Aβ vaccine). The third vaccine was made by adding the Fc portion of human immunoglobulins to the 3' end of the Aβ1-42 sequence to stabilize the secreted protein (Aβ-Fc vaccine). To prevent unwanted disulfide bonds, three cystines in the sequence were substituted with serine.

Transfection of DNA Vaccines and Western Blot Analysis. Three DNA vaccines were transfected to HEK293T cells and the amounts of produced Aβ peptide were measured by using ELISA. HEK293T cells in 60–70% confluence were prepared on 6-well plates (Costar, Cambridge, MA). The cells were first cultured in serum-free RPMI medium 1640 for 2 h with one of three DNA vaccines (K-Aβ, IgL-Aβ, or Aβ-Fc) and Lipofectamine PLUS reagent (Invitrogen). Then, the cells were cultured overnight in RPMI medium 1640 supplemented with 5% FBS for cellular stabilization and growth. For the Western blot analysis, the cells were again cultured in serum-free medium for an additional 8 h to remove unnecessary proteins.

Culture supernatants and cell pellets were harvested and run on NuPAGE 12% Bis-Tris gel (Invitrogen) and transferred to the PVDF membrane (Immobilon-P; Millipore). After blocking with 10% nonfat milk, the blots were incubated with 6E10 (anti-human Aβ1–17 antibody, 1:100; Abcam, Cambridge, U.K.) at 4°C for 1 h, followed by incubation with biotin-conjugated anti-mouse IgG (1:1,000; Vector Laboratories) for 1 h and with ABC-HRP (VectorLaboratories) for 1 h. The blots were developed by enhanced chemiluminescence reagents (Immunostar kit; Wako Biochemicals) according to the manufacturer's instructions.

Administration of the Vaccines. DNA vaccines (100 μg) and bupivacaine (0.25 mg) in 100 μl was administered i.m. on a weekly basis for 6 weeks (39). The vaccines without bupivacaine were injected biweekly thereafter. To examine the prophylactic effect, vaccination was started at 3–4 months of age, before amyloid plaque appearance. The therapeutic treatment was started at 12 months of age, after amyloid plaque appearance.

Immunohistochemistry. Mice were killed under deep anesthesia, and the brains were removed and immersion-fixed in 4% paraformaldehyde. Paraffin-embedded sections (6 μm) were stained immunohistochemically with mAb (6F/3D) against Aβ8–17 (DAKO), anti-CD5 mAb against T lymphocytes (BD Biosciences Pharmingen) and Mac-3 against mononuclear phagocytes (BD Biosciences Pharmingen). For 6F/3D staining, the sections were pretreated in formic acid for 3 min. The sections were then incubated in the primary antibody at a 1:200 dilution. After washing, the sections were incubated with biotinylated horse anti-mouse IgG (Vector Laboratories), followed by a horseradish peroxidase (HRP)-labeled Vectastain Elite ABC kit (Vector Laboratories). HRP-binding sites were detected in 0.005% diaminobenzidine and 0.01% hydrogen peroxide. CD5 (1:25) and Mac-3 (1:25) stainings were performed similarly, with overnight incubation of the primary antibodies.

Quantitative Analysis of Aβ Burden. Aβ burdens were quantitated in the cerebral cortex and hippocampus, according to the method described in ref. 40. All of the procedures were performed by an individual blind to the experimental condition of the study. The images under an Olympus Vanox microscope were captured with a 3 charge-coupled device Olympus digital camera. The amyloid load was measured in 10 fields from the cingulated to retrosplenial cortex in the left hemispheres of the mice (600 $\times$ 400 μm each), chosen randomly. Analysis in the hippocampus was performed on the entire hippocampus in a similar manner. Aβ depositions that occupied the field were expressed as pixels by using the NIH IMAGE software.

ELISA. Microtiter plates were coated with 2 μg/ml human Aβ1–40 (Peptide Institute, Osaka) in 0.1 M sodium carbonate buffer (pH 9.5) at 4°C overnight. After washing three times, plates were incubated for 2 h with serial dilutions of plasma samples in PBS in 12 rows of wells starting with 4-fold-diluted plasma (the greatest dilution tested was 1:213). The plates were washed and

IMMUNOLOGY

incubated with a 1,000-fold dilution of biotinylated anti-mouse IgG (Vector Laboratories), followed by incubation with 2-fold dilutions of Vectastain ABC-kit solution (Vector Laboratories). Bound antibodies were detected by using SIGMA FAST (Sigma-Aldrich), and the absorbance at 450 nm was read on an automated plate reader (Model 550; Bio-Rad). The antibody titer was defined as the reciprocal of the greatest dilution of plasma that gives half-maximal binding to Aβ, which was determined by dividing the highest OD_{450} value in the dilution range of each sample by 2.

T Cell-Proliferation Assay. The proliferative responses of draining lymph node cells were assayed in microtiter plates (Costar, Cambridge, MA) by the uptake of [^{3}H]thymidine. Aβ1-42 peptide (50 μg) emulsified with CFA (twice) and Fc-Aβ vaccine

(three times) was injected into APP23 mice or B6 mice, and then the drainage lymph nodes were taken 3 weeks after the first injection. Lymph node cells (2 × 10^5 cells per well) were cultured with 0.3–10 μM Aβ1-42 peptide for 3 days and subsequently pulsed for 18 h with 0.5 μCi (1 Ci = 37 GBq) of [^{3}H]thymidine (Amersham Pharmacia Biotech). Incorporation of [^{3}H]thymidine was measured by liquid scintillation spectrometry.

Statistical Analysis. Student's t test or Mann–Whitney's U test was used for the statistical analysis. Correlations between the antibody titer and the reduction of Aβ burden was estimated by the CORREL function.

1. Hardy, J. & Selkoe, D. J. (2002) *Science* **297**, 353–356.
2. Selkoe, D. J. & Schenk, D. (2003) *Annu. Rev. Pharmacol. Toxicol.* **43**, 545–584.
3. Schenk, D., Barbour, R., Dunn, W., Gordon, G., Grajeda, H., Guido, T., Hu, K., Huang, J., Johnson-Wood, K., Khan, K., et al. (1999) *Nature* **400**, 173–177.
4. Weiner, H. L., Lemere, C. A., Maron, R., Spooner, E. T., Grenfell, T. J., Mori, C., Issazadeh, S., Hancock, W. W. & Selkoe, D. J. (2000) *Ann. Neurol.* **48**, 567–579.
5. Bard, F., Cannon, C., Barbour, R., Burke, R. L., Games, D., Grajeda, H., Guido, T., Hu, K., Huang, J., Johnson-Wood, K., et al. (2000) *Nat. Med.* **6**, 916–919.
6. Janus, C., Pearson, J., McLaurin, J., Mathews, P. M., Jiang, Y., Schmidt, S. D., Chishti, M. A., Horne, P., Heslin, D., French, J., et al. (2000) *Nature* **408**, 979–982.
7. Morgan, D., Diamond, D. M., Gottschall, P. E., Ugen, K. E., Dickey, C., Hardy, J., Duff, K., Jantzen, P., DiCarlo, G., Wilcock, D., et al. (2000) *Nature* **408**, 982–985.
8. Hock, C., Konietzko, U., Papassotiropoulos, A., Wollmer, A., Streffer, J., von Rotz, R. C., Davey, G., Moritz, E. & Nitsch, R. M. (2002) *Nat. Med.* **8**, 1270–1275.
9. Orgogozo, J. M., Gilman, S., Dartigues, J. F., Laurent, B., Puel, M., Kirby, L. C., Jouanny, P., Dubois, B., Eisner, L., Flitman, S., et al. (2003) *Neurology* **61**, 46–54.
10. Nicoll, J. A., Wilkinson, D., Holmes, C., Steart, P., Markham, H. & Weller, R. O. (2003) *Nat. Med.* **9**, 448–452.
11. Wolff, J. A., Malone, R. W., Williams, P., Chong, W., Acsadi, G., Jani, A. & Felgner, P. L. (1990) *Science* **247**, 1465–1468.
12. Nishikawa, M. & Huang, L. (2001) *Hum. Gene. Ther.* **12**, 861–870.
13. Nishikawa, M. & Hashida, M. (2002) *Biol. Pharm. Bull.* **25**, 275–283.
14. Lobell, A., Weissert, R., Storch, M. K., Svanholm, C., de Graaf, K. L., Lassmann, H., Andersson, R., Olsson, T. & Wigzell, H. (1998) *J. Exp. Med.* **187**, 1543–1548.
15. Matsumoto, Y., Jee, Y. & Sugisaki, M. (2000) *J. Immunol.* **164**, 2248–2254.
16. Matsumoto, Y. (2000) *J. Neuroimmunol.* **110**, 1–12.
17. Robinson, W. H., Fontoura, P., Lee, B. J., de Vegvar, H. E., Tom, J., Pedotti, R., DiGennaro, C. D., Mitchell, D. J., Fong, D., Ho, P. P., et al. (2003) *Nat. Biotechnol.* **21**, 1033–1039.
18. Garren, H., Ruiz, P. J., Watkins, T. A., Fontoura, P., Nguyen, L. T., Estline, E. R., Hirschberg, D. L. & Steinman, L. (2001) *Immunity* **15**, 15–22.
19. Fernandez-Vizarra, P., Fernandez, A. P., Castro-Blanco, S., Serrano, J., Bentura, M. L., Martinez-Murillo, R., Martinez, A. & Rodrigo, J. (2004) *Histol. Histopathol.* **19**, 823–844.
20. Oddo, S., Caccamo, A., Kitazawa, M., Tseng, B. P. & LaFerla, F. M. (2003) *Neurobiol. Aging* **24**, 1063–1070.
21. Oddo, S., Caccamo, A., Shepherd, J. D., Murphy, M. P., Golde, T. E., Kayed, R., Metherate, R., Mattson, M. P., Akbari, Y. & LaFerla, F. M. (2003) *Neuron* **39**, 409–421.
22. Oddo, S., Billings, L., Kesslak, J. P., Cribbs, D. H. & LaFerla, F. M. (2004) *Neuron* **43**, 321–332.
23. Monsonego, A., Zota, V., Karni, A., Krieger, J. I., Bar-Or, A., Bitan, G., Budson, A. E., Sperling, R., Selkoe, D. J. & Weiner, H. L. (2003) *J. Clin. Invest.* **112**, 415–422.
24. Qu, B., Rosenberg, R. N., Li, L., Boyer, P. J. & Johnston, S. A. (2004) *Arch. Neurol.* **61**, 1859–1864.
25. Monsonego, A., Maron, R., Zota, V., Selkoe, D. J. & Weiner, H. L. (2001) *Proc. Natl. Acad. Sci. USA* **98**, 10273–10278.
26. Yamamoto, S., Yamamoto, T., Kataoka, T., Kuramoto, E., Yano, O. & Tokunaga, T. (1992) *J. Immunol.* **148**, 4072–4076.
27. Krieg, A. M., Yi, A. K., Matson, S., Waldschmidt, T. J., Bishop, G. A., Teasdale, R., Koretzky, G. A. & Klinman, D. M. (1995) *Nature* **374**, 546–549.
28. Klinman, D. M., Yi, A. K., Beaucage, S. L., Conover, J. & Krieg, A. M. (1996) *Proc. Natl. Acad. Sci. USA* **93**, 2879–2883.
29. Gelman, A. E., Zhang, J., Choi, Y. & Turka, L. A. (2004) *J. Immunol.* **172**, 6065–6073.
30. Matsumo, Y., Sakuma, H., Miyakoshi, A., Tsukada, Y., Kohyama, K., Park, I. & Tanuma, N. (2005) *J. Neuroimmunol.* **170**, 49–61.
31. Beccaccio, G. L., Mor, F. & Steinman, L. (1999) *Int. Immunol.* **11**, 289–296.
32. Quintana, F. J., Rotem, A., Carmi, P. & Cohen, I. R. (2000) *J. Immunol.* **165**, 6148–6155.
33. Zhang, J., Wu, X., Qin, C., Qi, J., Ma, S., Zhang, H., Kong, Q., Chen, D., Ba, D. & He, W. (2003) *Neurobiol. Dis.* **14**, 365–379.
34. Hara, H., Monsonego, A., Yuasa, K., Adachi, K., Xiao, X., Takeda, S., Takahashi, K., Weiner, H. L. & Tabira, T. (2004) *J. Alzheimers Dis.* **6**, 483–488.
35. Sturchler-Pierrat, C., Abramowski, D., Duke, M., Wiederhold, K. H., Mistl, C., Rothacher, S., Ledermann, B., Burki, K., Frey, P., Paganetti, P. A., et al. (1997) *Proc. Natl. Acad. Sci. USA* **94**, 13287–13292.
36. Sturchler-Pierrat, C. & Staufenbiel, M. (2000) *Ann. N.Y. Acad. Sci.* **920**, 134–139.
37. Moechars, D., Lorent, K., de Strooper, B., Dewachter, I. & van Leuven, F. (1996) *EMBO J.* **15**, 1265–1274.
38. Calhoun, M. E., Wiederhold, K. H., Abramowski, D., Phinney, A. L., Probst, A., Sturchler-Pierrat, C., Staufenbiel, M., Sommer, B. & Jucker, M. (1998) *Nature* **395**, 755–756.
39. Danko, I., Fritz, J. D., Jiao, S., Hogan, K., Latendresse, J. S. & Wolff, J. A. (1994) *Gene Ther.* **1**, 114–121.
40. Sigurdsson, E. M., Scholtzova, H., Mehta, P. D., Frangione, B. & Wisniewski, T. (2001) *Am. J. Pathol.* **159**, 439–447.

ELSEVIER

Neuroscience
Letters

Increased phosphorylation of caveolin-1 in the spinal cord of Lewis rats with experimental autoimmune encephalomyelitis

Heechul Kim[a], Meejung Ahn[a], Jeeyoung Lee[a], Changjong Moon[a], Yoh Matsumoto[b], Chang Sung Koh[c], Taekyun Shin[a],*

[a] Department of Veterinary Medicine, Cheju National University, Jeju 690-756, South Korea
[b] Department of Molecular Neuropathology, Tokyo Metropolitan Institute for Neuroscience, Fuchu, Tokyo 183, Japan
[c] Department of Biomedical Laboratory Sciences, Shinshu University School of Health Sciences, 3-1-1 Asahi, Matsumoto 390-8621, Japan

Abstract

The expression of phospho-specific caveolin-1 (p-caveolin-1) was analyzed in the spinal cord of Lewis rats with experimental autoimmune encephalomyelitis (EAE). Western blot analysis showed that p-caveolin-1 was constitutively expressed in normal spinal cords and that it significantly increased in the spinal cord with EAE at both early and peak stages of EAE ($P < 0.05$), and decreased slightly at the recovery stage of EAE. Immunohistochemistry showed that p-caveolin-1 was constitutively expressed in few vascular endothelial cells and glial cells in the spinal cords of normal rats. In EAE lesions, p-caveolin-1 was intensely immunostained in inflammatory T cells and macrophages. Therefore, we postulate that phosphorylation of caveolin-1 occurred in the inflammatory cells of EAE lesions, and that caveolin-associated cell activation is mainly associated with inflammatory cells that appear during early and peak stages of EAE.
© 2006 Elsevier Ireland Ltd. All rights reserved.

Keywords: Caveolin-1; Experimental autoimmune encephalomyelitis; Glial cells; Macrophages

Caveolin-1 is a structural protein of caveolae, which are flask-shaped vesicular invaginations of the plasma membrane with diameters of 50–100 nm [4,8]. Caveolin is a transmembrane adaptor molecule that recognizes glycosylphosphatidyl inositol (GPI)-linked proteins and interacts with downstream cytoplasmic signaling molecules such as Src-family tyrosine kinases and hetero-trimeric G proteins [9,10]. Caveolin is abundant in a variety of cell types including adipocytes, endothelial cells, smooth muscle cells [8], macrophages [3,7], astrocytes [5,13], and differentiating PC 12 cells [2], possibly mediating signal transduction. Under certain activation conditions, caveolin is phosphorylated, and the phosphorylation of caveolin at Tyr-14, Ser-88, and other residues in v-Src-transformed cells leads to flattening, aggregation, and fusion of caveolae and caveolae-derived vesicles [9]. Phosphorylation of caveolin affects the cell shape, which is an important finding in the activation and migration of inflammatory cells.

Experimental autoimmune encephalomyelitis (EAE) is an experimentally induced autoimmune disease of the central nervous system (CNS) mediated by CD4+ T cells, which is used as an animal model of multiple sclerosis, a human demyelinating disease [11]. EAE lesions are characterized by the infiltration of T cells and macrophages into the subarachnoid space during the early stage and the activation of microglia and astrocytes during the peak symptomatic stage of the disease [14]. In a previous study, we found that caveolins significantly increase in the spinal cord with EAE [13], but little is known about the phosphorylation state of caveolin-1. The goal of the present study was to examine the expression of phospho-specific caveolin-1 (p-caveolin-1) and to localize its expression in spinal cords with EAE.

Lewis rats were obtained from Harlan (Indianapolis, IN, USA) and were bred in our animal facility. Female rats aged 7–12 weeks and weighing 160–200 g were used in the experiments. All experiments were carried out using accepted ethical guidelines. The footpads of both hind feet of the rats in the EAE group were injected with 100 μl of an emulsion containing equal parts of myelin basic protein (1 mg/ml) and complete Freund's

* Corresponding author. Tel.: +82 64 754 3363; fax: +82 64 756 3354.
E-mail address: shint@cheju.ac.kr (T. Shin).

adjuvant (CFA) supplemented with Mycobacterium tuberculosis H37Ra (5 mg/ml; Difco, Detroit, MI, USA). The rats in the control group were immunized with CFA only. After the injections, the rats were observed daily for clinical signs of EAE. The progression of EAE was divided into seven clinical stages: Grade 0 (G0), no signs; G1, floppy tail; G2, mild paraparesis; G3, severe paraparesis; G4, tetraparesis; G5, moribund condition or death; and R0, the recovery stage.

Rabbit polyclonal anti-p-caveolin-1 (Tyr-14, catalog #sc-14037-R; Santa Cruz Biotechnology, Santa Cruz, CA, USA) and mouse monoclonal anti-beta-actin (Sigma, St. Louis, MO, USA) antibodies were used in this study. To identify cell phenotypes, the following monoclonal antibodies were used; mouse monoclonal anti-glial fibrillary acidic protein (anti-GFAP; Sigma), ED1 (mouse monoclonal anti-rat macrophage; Serotec, London, UK), R73 (mouse monoclonal anti-T cell receptor $\alpha\beta$; Blackthorn, Bicester, UK), OX1 (anti-leukocyte common antigen CD45; Serotec), OX42 (anti-complement receptor type 3; Serotec) antibodies. Biotinylated isolectin B4 (IB4) derived from Griffonia simplicifolia (Sigma) was used to show vascular endothelial cells [16] and activated microglia/macrophages.

In this study, spinal cords were sampled on Days 9–11, 12–15, and 21 post-immunization (p.i.), which coincided with the early (G1), peak (G3), and recovery stages (R0) of EAE, respectively. The spinal cords of normal rats were used as controls. At each sampling, five rats from each group were sacrificed under deep anesthesia, and pieces of the lumbar spinal cords were collected. Spinal cord samples were processed for paraffin embedding after fixation in 4% paraformaldehyde in phosphate-buffered saline (PBS, pH 7.4) or quick-frozen and stored for later use in immunoblotting. To prepare frozen sections, pieces of the lumbar spinal cords were snap-frozen in optimal cutting temperature (OCT) compound (Sakura, Tokyo, Japan) and stored at $-80\,^{\circ}\mathrm{C}$ until use. Sections (8 μm thick) were cut in a cryostat (Leica, Nussloch, Germany).

The spinal cord tissue was homogenized in modified radioimmunoprecipitation assay (RIPA) buffer (20 mM Tris, pH 7.5, 150 mM NaCl, 1% Triton-X 100, 0.5% sodium deoxycholate, 0.1% sodium dodecyl sulfate (SDS), 1% NP-40, 10 mM NaF, 1 mM EDTA, 1 mM EGTA, 1 mM Na_3VO_4, 1 mM PMSF, 10 μg/ml aprotinin, and 10 μg/ml leupeptin) with 20 strokes in a homogenizer. The homogenates were transferred to microtubes and centrifuged at 14,000 rpm for 20 min, and the supernatant was harvested. For the immunoblot assay, supernatant containing 40 μg of protein was loaded into each lane of 12% SDS–PAGE gels, electrophoresed, and immunoblotted onto nitrocellulose membranes (Schleicher and Schuell, Keene, NH, USA). The residual binding sites on the membrane were blocked by incubation with 5% nonfat milk in Tris-buffered saline (TBS; 10 mM Tris–HCl (pH 7.4) and 150 mM NaCl) for 1 h, and then incubated with rabbit polyclonal anti-p-caveolin-1 (Tyr-14) antibody for 2 h.

The blots were washed three times in TBS containing 0.1% Tween-20 and then incubated with horseradish peroxidase-conjugated anti-rabbit IgG (Vector, Burlingame, CA, USA) for 1 h. The bound antibody was detected using enhanced chemiluminescence (ECL) reagents (Amersham, Arlington Heights, IL,

USA) according to the manufacturer's instructions. After imaging, the membranes were stripped and reprobed using monoclonal anti-beta-actin antibody as the primary antibody (Sigma). The density (OD/mm^2) of each band was measured with a scanning laser densitometer (GS-700; Bio-Rad, Hercules, CA, USA) and was reported as the mean ± S.E. The ratios of the density of p-caveolin-1 band to that of the beta-actin band were compared using Molecular Analyst software (Bio-Rad). The results were analyzed statistically by one-way analysis of variance (ANOVA) followed by the post hoc Student–Newman–Keul's t-test for multiple comparisons. In all cases, $P < 0.05$ was considered significant.

Briefly, paraffin-embedded spinal cord sections (5 μm) were deparaffinized, treated with citrate buffer (0.01 M, pH 6.0) in a microwave for 3 min, and then treated with 0.3% hydrogen peroxide in methyl alcohol for 20 min to block endogenous peroxidase activity. After three washes with PBS, the sections were incubated with 10% normal goat serum, and then incubated for 1 h at room temperature with primary antibodies including rabbit polyclonal anti-p-caveolin-1. Immunoreactivity was visualized with an avidin–biotin peroxidase complex (Vector Elite; Vector). The peroxidase reaction was developed using a diaminobenzidine substrate kit (Vector).

To examine the cell phenotype of p-caveolin-1 expression, double immunofluorescence was applied. First, paraffin sections were reacted with primary rabbit anti-p-caveolin-1 and followed by fluorescein isothiocyanate (FITC)-labeled goat anti-rabbit IgG (Sigma, St. Louis, MO, USA). Then, the slides were incubated with second primary reagent including ED1 and anti-GFAP, and sequentially reacted with tetramethyl rhodamine isothiocyanate (TRITC)-labeled goat anti-mouse IgG (Sigma). For the labeling of p-caveolin-1 and either OX1, OX42 or R73, frozen sections were used. The frozen sections were air-dried, fixed in 4% paraformaldehyde in phosphate-buffered saline (PBS) (pH 7.4) for 20 min, and hydrated. Then, the slides reacted with rabbit anti-p-caveolin-1 were reacted biotinylated anti-rabbit IgG (Vector), followed by TRITC-labeled streptavidin (Zymed, San Francisco, CA, USA), and then secondary primary antibodies including OX1, OX42 or R73 and sequentially reacted with FITC-labeled goat anti-mouse IgG (Sigma). To see the co-localization of p-caveolin-1 and IB4 in EAE lesions, sections were reacted with biotinylated IB4 (Sigma), followed by TRITC-labeled streptavidin (Zymed, San Francisco, CA, USA). And then, secondary primary anti-p-caveolin-1 was reacted and followed by FITC-labeled goat anti-rabbit IgG (Sigma). To reduce or eliminate lipofuscin autofluorescence, the sections were washed in PBS (three times for 1 h) at RT, then dipped briefly in distilled H_2O, treated with 10 mM $CuSO_4$ in ammonium acetate buffer (50 mM CH_3COONH_4, pH 5.0) for 20 min, dipped briefly again in distilled H_2O, and returned to PBS. The double immunofluorescence-stained specimens were examined with an FV500 laser confocal microscope (Olympus, Tokyo, Japan).

The level of p-caveolin-1 was semiquantitatively evaluated in the spinal cord during the course of EAE using Western blot analysis. The expression of p-caveolin-1 immunoreactivity was detected at low levels in the spinal cords of normal control rats